GEND-INF-
March

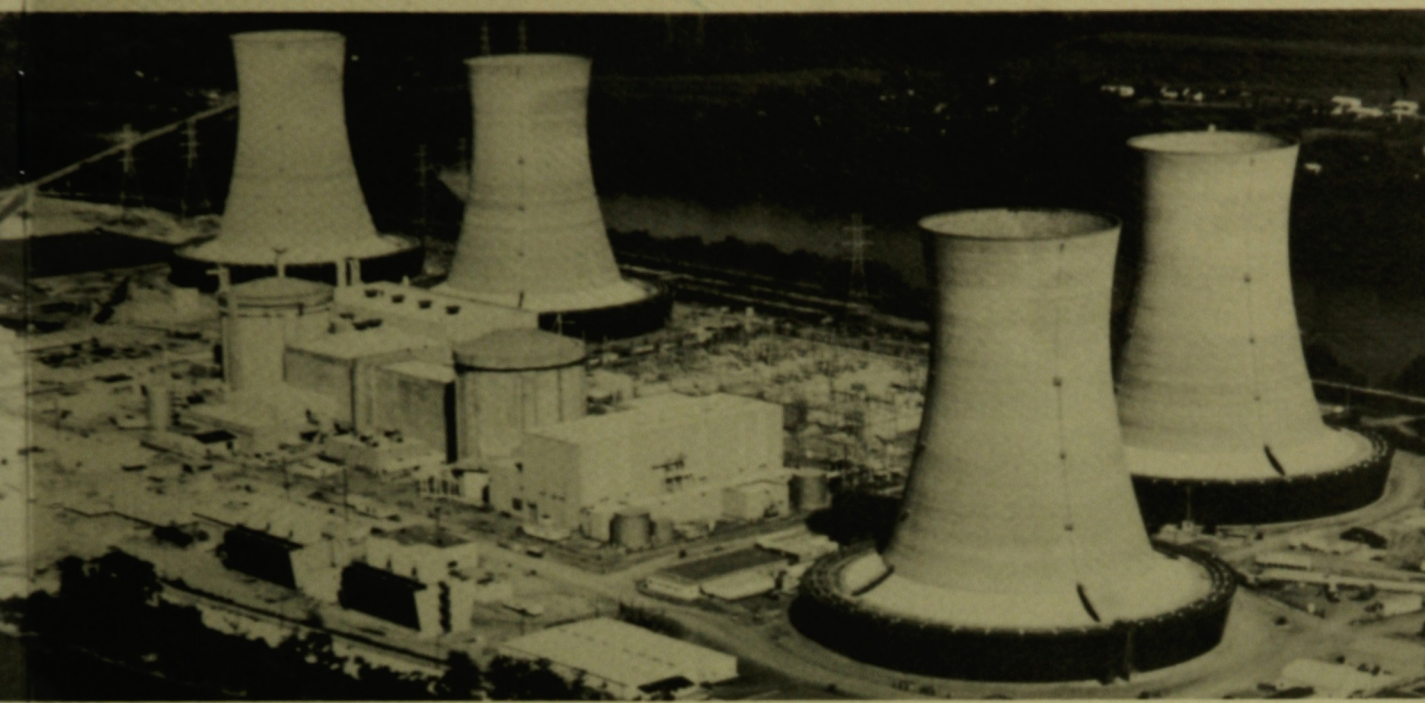

This is an informal report intended for use as a preliminary or working document

GEND

General Public Utilities • Electric Power Research Institute • U.S. Nuclear Regulatory Commission • U.S. Department of Energy

EXAMINATION OF THE LEADSCREW SUPPORT TUBE FROM THREE MILE ISLAND REACTOR UNIT 2

M. P. Failey
V. Pasupathi
M. P. Landow

M. J. Stenhouse
J. Ogden
R. S. Denning

Prepared for the
U.S. Department of Energy
Three Mile Island Operations Office
Under Contract No. DE-AC07-76ID01570

GEND-INF-067

EXAMINATION OF THE LEADSCREW SUPPORT TUBE FROM THREE MILE ISLAND REACTOR UNIT 2

M. P. Failey
V. Pasupathi
M. P. Landow
M. J. Stenhouse
J. Ogden
R. S. Denning

Published March 1986

Battelle Columbus Laboratories
505 King Avenue
Columbus, Ohio 43201

Prepared for EG&G Idaho, Inc.
and the U.S. Department of Energy
Three Mile Island Operations Office
Under DOE Contract No. DE-AC07-761D01570

ABSTRACT

A short section of leadscrew support tube H8 from the Three Mile Island Unit 2 reactor was examined. The primary objective of the examination was to characterize surface deposits on the section with respect to chemical and radiochemical concentrations. This was accomplished by removal, separation, and dissolution of the deposits and analysis by secondary ion mass spectrometry, electron spectroscopy for chemical analysis, inductively coupled argon plasma spectrometry, and x-ray diffraction techniques. In addition, the deposits were studied using metallographic and scanning electron microscopic techniques. Studies on effectiveness of various decontamination solutions also were performed. Results, in general, were consistent with data obtained in previous examinations of pieces of leadscrew.

EXECUTIVE SUMMARY

A small section (approximately 9-cm long) of leadscrew support tube H8 from the Three Mile Island Unit 2 (TMI-2) reactor was examined at Battelle Columbus Laboratories. The primary objective of the examination was to characterize the surface deposits observed on the section. Information obtained from this examination will become a part of the body of data needed for understanding radionuclide behavior during severe core damage accidents.

Examinations conducted on the leadscrew support tube (LST) section included detailed chemical, structural, and radiochemical analyses, using a variety of analytical techniques. In addition, a decontamination effectiveness study involving five different decontamination solutions was conducted. Results of this task should be useful for reactor decontamination and other recovery operations at TMI-2.

Results of the examinations and conclusions derived therefrom are as follows:

- Visual examination of the LST section showed the presence of metallic particles at the bottom end of the section.

- Gamma-activity scanning showed relatively flat activity over the length of the section. The primary sources of gamma activity were Cs-134 and Cs-137. No other gamma emitters were identified on the LST surfaces. Other isotopes identified in the loose debris from the packaging included Co-60, Sb-125, and Ce-144.

- Some of the surface deposits were found to be loosely adherent and easily transferred to materials coming in contact with the LST section. Metallographic examination of specimens from the section showed the presence of two separate and identifiable layers: loosely adherent and tightly adherent. The loosely

adherent deposit on the inner surface appeared to be more porous and less uniform in thickness than that on the outer surface. The outer surface deposits exhibited numerous bright, metallic particles, while the inner surface deposits had few or none.

- Elemental analysis of specimens from the LST section indicated the following:

  - No fission product cesium was detectable in the deposits using the scanning electron microscope, even though cesium was the primary source of radioactivity in the LST. It appears that the specific activities of Cs-134 and Cs-137 are very high, and the elemental concentration of cesium was not high enough to be detectable.

  - Most of the inner and outer surface deposits appeared to contain iron and chromium in varying amounts. Very few isolated particles were observed containing U, Zr, or Sn.

  - The metallic particles observed at the bottom end of the section and in the outer surface deposits contained varying amounts of Ag, In, and Cd.

  - X-ray diffraction studies of the deposits showed compounds containing iron and nickel. Trace concentrations of silver also were observed.

  - Electron spectroscopy for chemical analysis showed the presence of Fe, Ag, In, Cd, and B in the outer surface deposits. No iodine was detected. Traces of cesium and tellurium were observed. The inner surface deposits showed only Fe, Cr, Ni, and O. This observation is consistent with the absence of metallic particles.

- Results from secondary ion mass spectroscopy showed the presence of a number of elements, including Cs, I, U, and Zr. There appeared to be no systematic variation in concentrations of these elements with respect to the depth profile.

- The microstructural appearance of the base metal of the LST section showed carbide precipitates in the grain boundary. It is believed that the LST may have experienced temperatures in the range of from 510 to 732°C (950 to 1350°F) during the accident.

- Results from the examination of the LST section are, in general, consistent with those from the leadscrew examinations. The total mass of fission products deposited on the LST surface is a very small fraction of the mass of fission products released from the core. The extent of deposition may have been higher during the accident; if so, it has been reduced by subsequent washing.

- Control rod material (Ag-In-Cd) appears to have been transported in the molten/vaporized state and subsequently deposited on the upper plenum surfaces.

Results obtained from examining the LST section are largely consistent with data obtained in previous examinations of pieces of leadscrew. The data should be considered supplementary to that obtained from the leadscrew examinations with respect to radionuclide transport and deposition during the accident.

CONTENTS

FIGURES

TABLES

EXAMINATION OF THE LEADSCREW SUPPORT TUBE FROM THREE MILE ISLAND REACTOR UNIT 2

1. INTRODUCTION

One of the major objectives of the technical data acquisition program for the Three Mile Island Unit 2 (TMI-2) reactor is to provide information on the release, transport, and deposition of fission products and other radionuclides during severe core damage accidents. This information is being obtained by detailed characterization of deposits on surfaces within the TMI-2 reactor coolant system that were uncovered during the accident. Results of these studies will be used to determine radionuclide source term values applicable to severe core damage accident conditions and to support reactor decontamination and other recovery operations.

One approach to obtaining data on the surface deposits is to remove samples containing the deposits and analyze them offsite. As part of this effort, sections of control rod leadscrew have been examined by several organizations to characterize surface deposits. Complementary to these examinations is the characterization by Battelle Columbus Laboratories of a section from the H8 leadscrew support tube (LST). This section, which is a sample of the surface immediately above the plenum assembly of the reactor (Figure 1), is a key to understanding fission product behavior in the upper part of the reactor vessel.

This report describes the examinations conducted on the section of leadscrew support tube and presents an evaluation of the results obtained. Also included are recommendations for follow-on work.

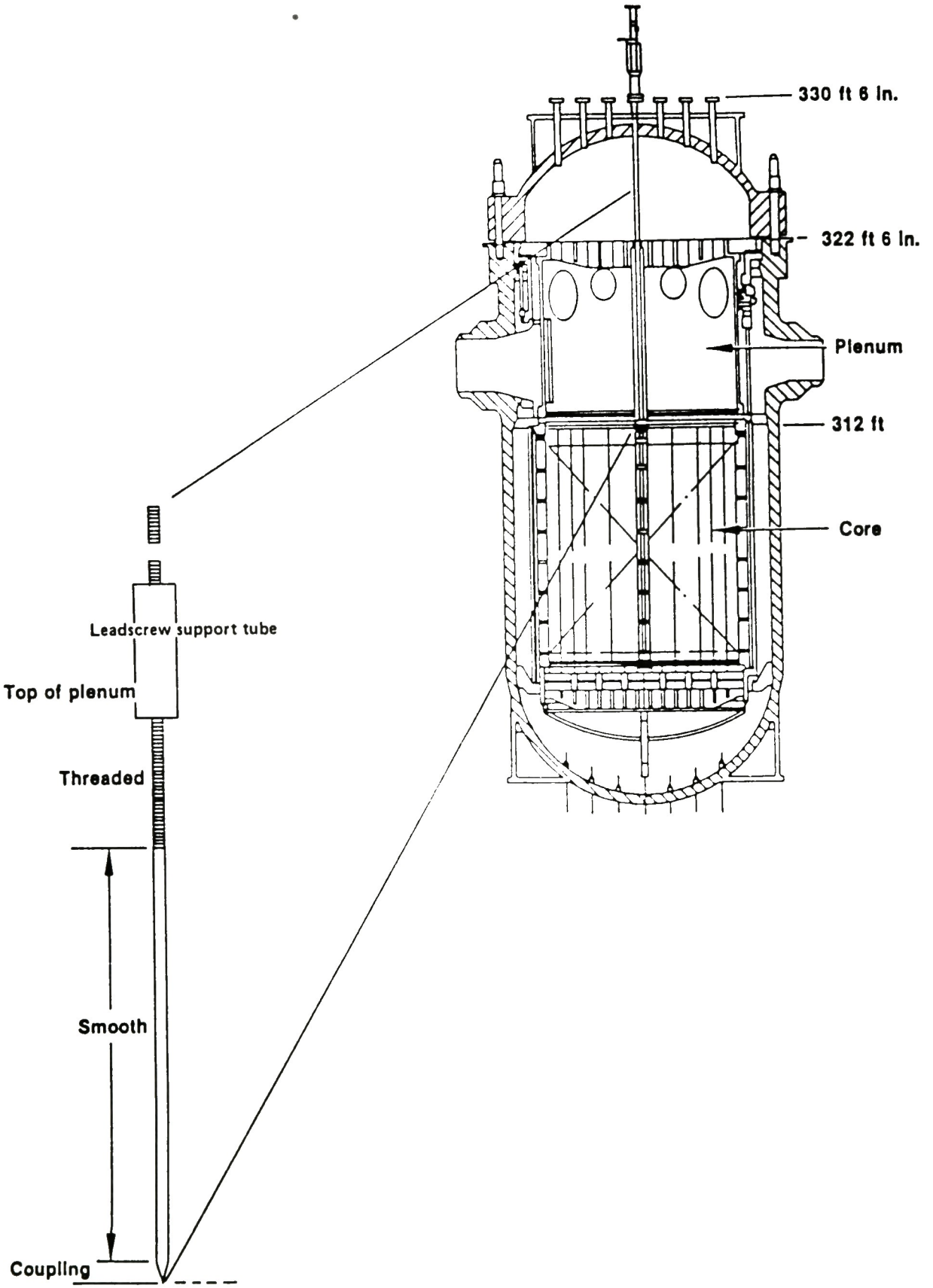

Figure 1. Schematic of the TMI-2 reactor core, showing location of the LST section.

2. EXAMINATIONS AND RESULTS

The examinations conducted on the section of LST included visual and photographic examinations; gamma-ray profiling; elemental and structural analysis of the surface deposits; decontamination effectiveness studies; radiochemical analysis, including measurement of I-129; and microstructural examination of the base metal.

2.1 Receipt and Initial Inspection

2.1.1 Visual and Photographic Examination

The LST section was shipped from the Babcock and Wilcox Lynchburg Research Center and received at the Battelle Hot Cell Facility in August 1984. The section was packaged in a yellow plastic bag and placed inside a lead shield approximately 3.8-cm-thick. The lead shield was further contained and centered in a 55-gal. drum.

The LST section was removed from the plastic bag for visual inspection and photographic documentation of its surface appearance. The inspection was performed in an open area outside the hot cells. Airflow was established over the section and vented away from personnel in the area to minimize the spread of any airborne contamination. All personnel in the area were equipped with personal airborne particulate sampling systems. Later analysis of the particulate filters indicated that no airborne activity was present during the examination period.

Radiation readings were taken on the LST section after it had been placed on an absorbent, white surface for photographic examination. The contact, beta-gamma radiation field was measured at 35 R/h, and the reading at 1 m was 70 mR/h.

The entire outside surface of the section was photographed in color. Most of the surface appeared solid black. The deposits appeared to be thin and largely uniform, with no evidence of distinguishable single particles

on the outside or inside cylindrical surfaces. Portions of the outer surface on one side were partially covered by a thin, yellow-orange deposit. The LST section and colored deposits are shown in Figure 2. The flat bottom of the section, which had been oriented toward the reactor core in service, showed evidence of metallic particles ranging in size from barely visible to about 1 mm in diameter, with the larger particles appearing spherical. Figure 3 is a photograph showing the inside surface of the section, which appeared black, similar to most of the outside surface. Some small areas of yellow-orange surface material also were observed, but these areas were less extensive than those found on the outside surface.

It was observed that the surface material was very easily transferred to objects coming in contact with the LST section, as shown by the presence of a partial, black ring on the white surface in front of the section (see Figure 2). The ring is residual material left behind when the section was moved to another position. The material was easily transferred to rubber surgical gloves coming in contact with the section. The transferred material was very radioactive.

Dimensional measurements were made of the LST section. The length, as measured on the short side, was 8.6 cm. The long side measured 9.5 cm, and the outside diameter was measured at 6.5 cm. After the initial inspection, the section was rebagged in polyethylene and transferred back to the lead shield, pending further studies.

The yellow plastic bag that had contained the section was packaged in a polyethylene bag and transferred to a glove box for recovery of the loose debris. Once inside the box, the bag was opened and unfolded. No large particles such as metal shavings or collectable loose powder were found in the bag; only a thin coating of black material was found where the bag had been in direct contact with the LST section. Some of the material was collected by scraping with a nickel spatula. It is likely that some plastic from the bag was collected with the surface material, because the bag itself showed evidence of radiation degradation by breaking apart and

Figures 2 and 3

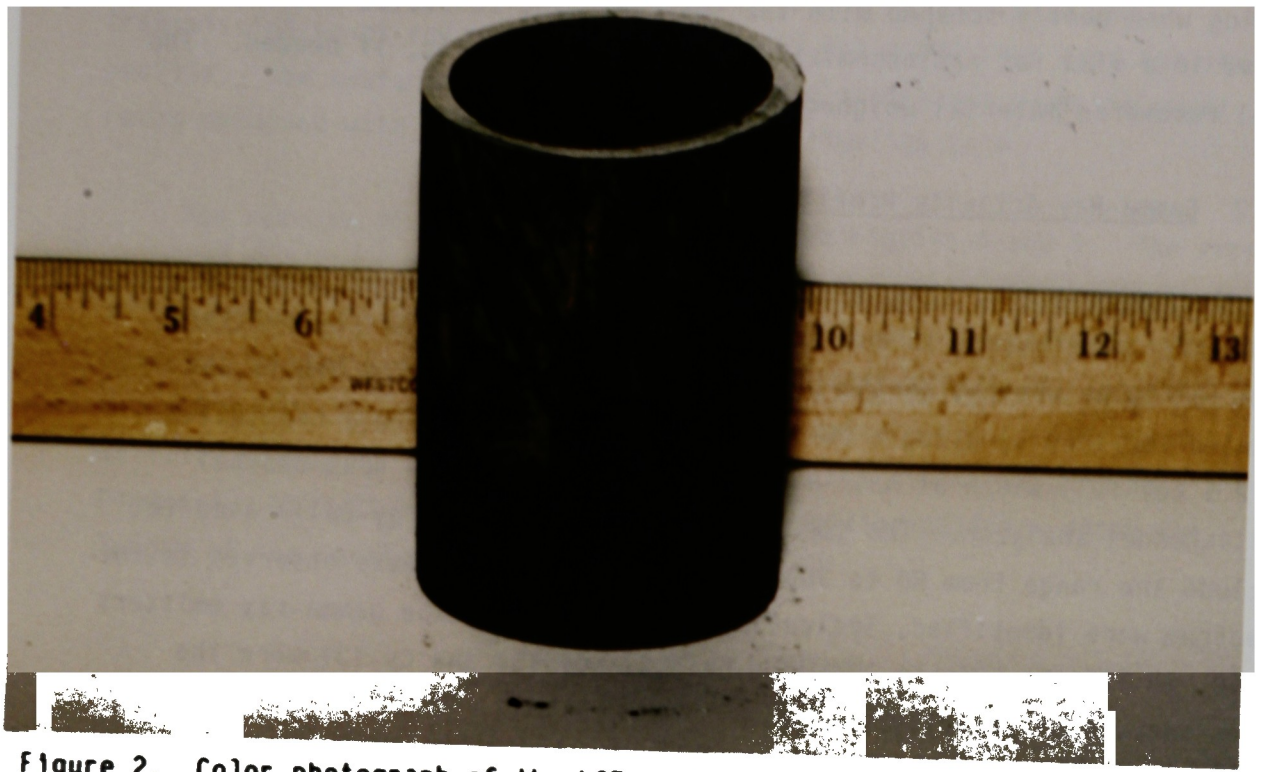

Figure 2. Color photograph of the LST section, showing yellow deposit on the outer surface.

Figure 3. Color photograph showing the inside surface of the LST section.

flaking when gently scraped with the spatula. The collected material was placed in a vial for radiochemical and chemical analysis, if needed. The total recovered material weighed about 15 mg.

2.1.2 Gamma-Ray Activity Profiling

The loose debris scraped from the packaging material was analyzed by gamma-ray spectroscopy to qualitatively identify all gamma-ray emitters expected to be present on the LST. The vial containing the debris was counted for 1800 s, using a 50-cm^3 germanium detector with a resolution of 2.5 keV full-width at half-maximum at 1332 keV, and a 4096-channel multichannel analyzer. The spectroscopy system was energy-calibrated to include the range from 80 to 2000 keV. All gamma-ray peaks observed in the spectrum were identified, indicating the presence of the gamma-ray emitters Co-60, Sb-125, Cs-134, Cs-137, and Ce-144. Cs-134 and Cs-137 were the major sources of activity.

The LST section was double bagged in polyethylene and transferred to a gamma-ray counting system for an axial activity scan. The counting system consisted of the same upward-looking, 50-cm^3 germanium detector used for the gamma-ray analysis of the loose debris. However, the system was modified so the LST section was positioned above the detector, with 10 cm of lead shielding between the section and the detector. A 0.32-cm hole was drilled through the lead shield to provide a port for the detector to view the section. The edge of the section was placed over the 0.32-cm hole. Beginning with the edge, a gamma-ray spectrum was accumulated for each axial 0.3-cm increment, as the LST section was moved past the port. Two axial scans were performed, one along the short (8.6-cm) side and the other along the long (9.5-cm) side of the section.

The integrated peak areas for the 662-keV line of Cs-137 and the 796-keV line of Cs-134 were used to measure the relative activities along the length of the section. The peak areas were corrected for background and shine from gamma rays penetrating the lead shield to the detector. The shine correction was performed by placing the section to the side of the

0.32-cm collimation hole, then accumulating data to determine the transmission count rates of the 662- and 796-keV gamma rays used for the profile. The measured shine count rates were subtracted from the count rates obtained with the section over the collimation hole.

The results of the two scans are shown in Figures 4 and 5. The zero position on the abscissa at the left side of each plot corresponds to the bottom end of the section, which pointed to the core in service. Each position increment corresponds to moving the section past the port by 0.3 $\pm$ 0.1 cm. Examination of Figure 5 shows a trend toward increased activity moving up the LST section; however, this is not evident in Figure 4. Variations in relative gamma-ray emitter activity along the length of the section are about 8%.

2.2 Tube Sectioning

After the gamma-ray scans, the LST section was transferred to the hot machining area. A band saw, cleaned to remove loose contamination and equipped with a new blade, was used to cut the section into rings. The LST section was cut perpendicular to the cylindrical axis, producing seven rings ranging in thickness from approximately 0.6 cm to approximately 3.8 cm. The first ring, cut from the bottom of the LST section, was designated Ring 1; and each subsequent ring was numbered sequentially up to 7. As each ring was cut, it was packaged in polyethylene and transferred to a lead shield for storage. Rings 3 and 7 were archived for possible future study.

Rings 1, 2, 4, 5, and 6 were transferred individually to a glove box and cut into specimens for the various studies. A hacksaw with a new blade was used, and the rings were held firmly in place with a small vise.

Specimens from the rings were designated with a specimen code of the form X-Y, where X represents the ring number and Y represents the specimen number (e.g., "Specimen 1-7" refers to the seventh specimen cut from Ring 1). If specimens with the X-Y designation were subsectioned further,

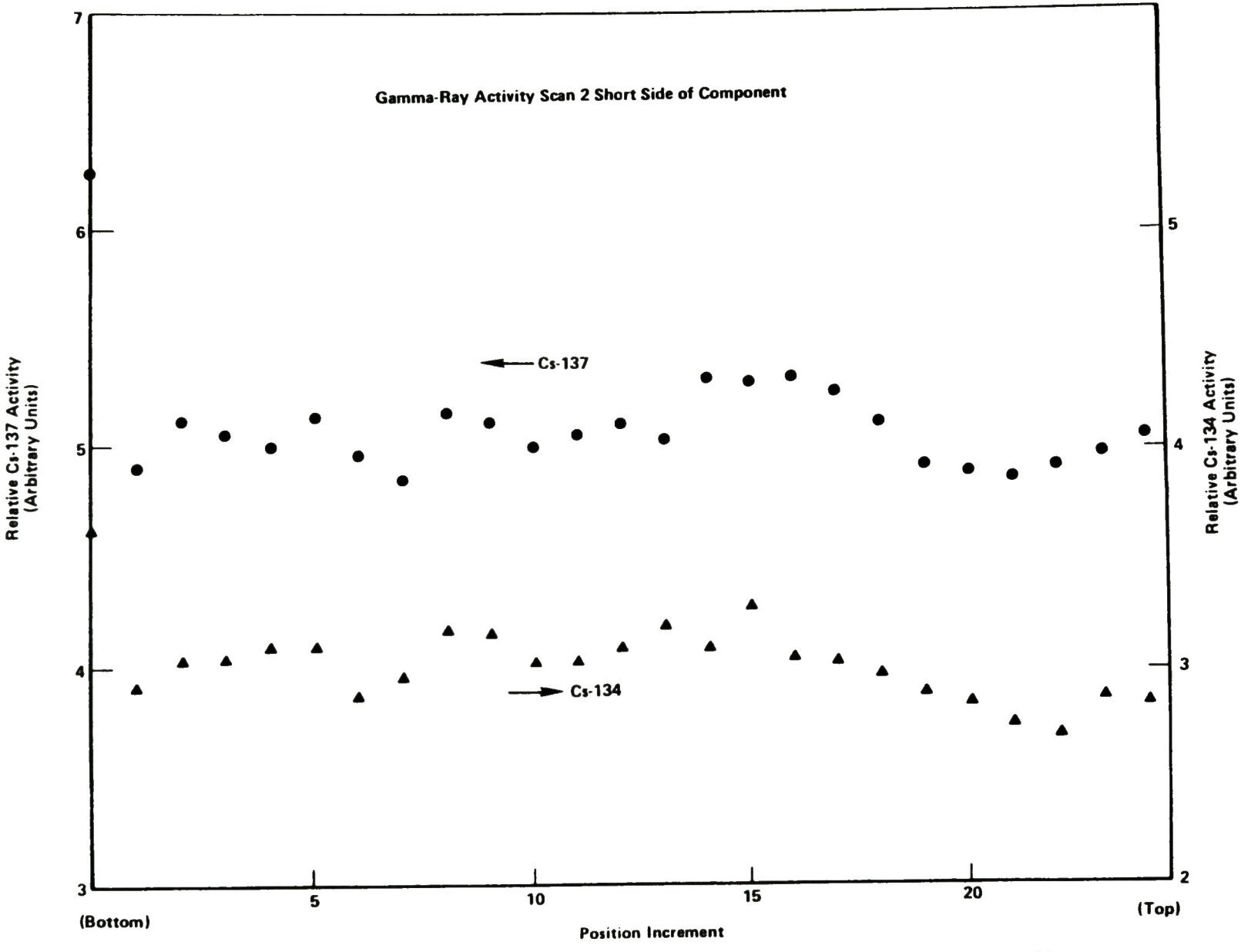

Figure 4. Gamma-ray activity scan along the short side of the LST section.

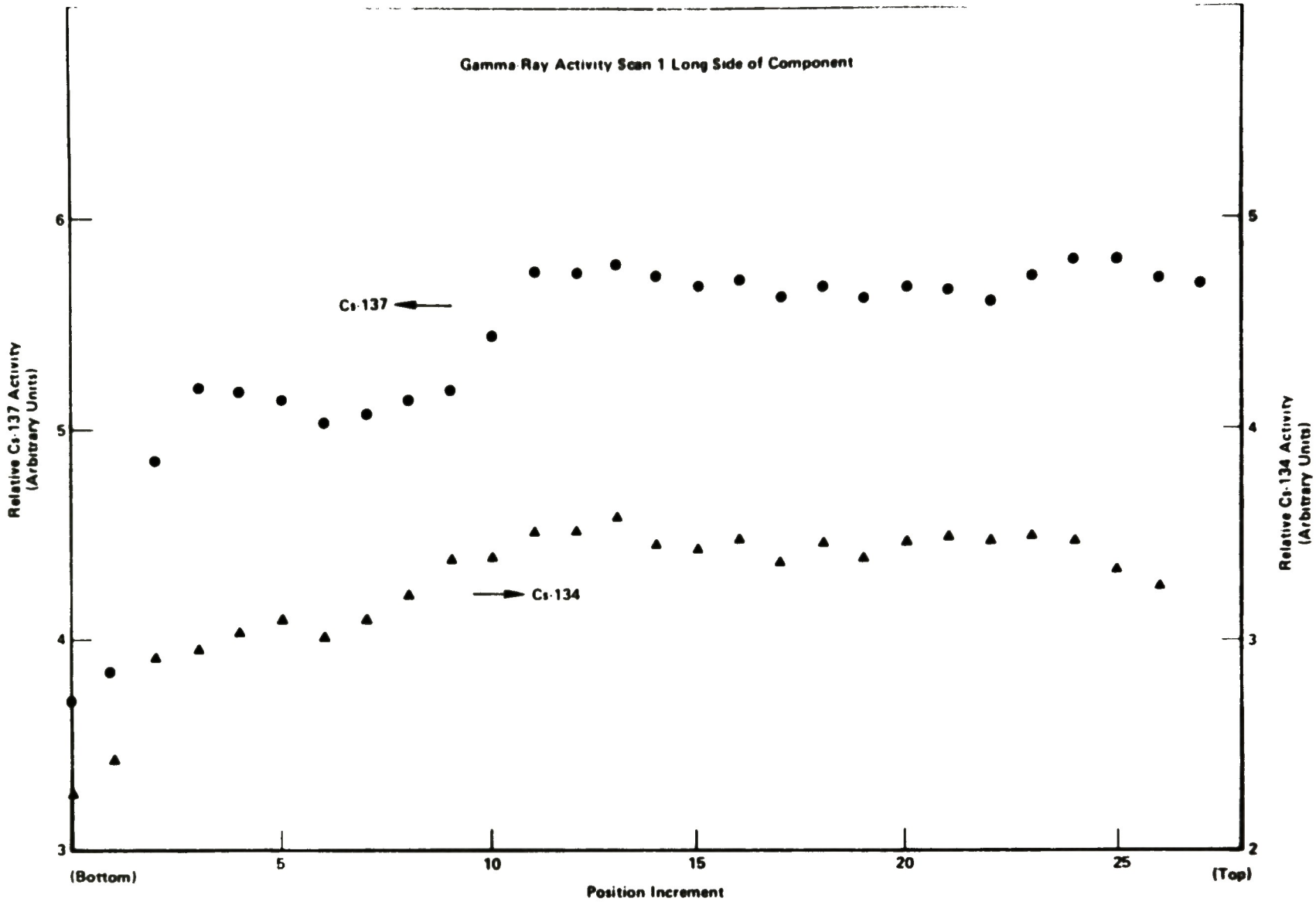

Figure 5. Gamma-ray activity scan along the long side of the LS1 section.

the resulting samples were designated with a code in the form X-Y.Z, with Z representing the number of the sample. The first sample cut from Specimen 1-7, for example, would be identified as Sample 1-7.1. All cutting operations were documented so that absolute locations on the LST section could be determined. As the specimens and samples were prepared, they were transferred through the air lock of the glove box to clean plastic vials.

2.3 Chemical and Radiochemical Analysis of Surface Deposits

2.3.1 Decontamination Effectiveness Studies

To assess the effectiveness of five solutions in removing the surface activity from the LST section, a series of decontamination tests was performed. The five solutions were the same as those used at TMI for initial chemical characterization of the surface deposits on a 30-cm section of leadscrew.[1]

The decontamination effectiveness tests were performed using small samples taken from neighboring locations on the LST section. Each sample had approximately equal inner- and outer-diameter surface areas, with a total contaminated surface area in the range of from 0.1 to 0.2 cm^2 per sample. All samples had both tightly and loosely adherent surface deposits.

2.3.1.1 Initial Tests of Five Decontamination Solutions. Before beginning the tests, all samples were analyzed by gamma-ray spectroscopy. This was done to determine activities so that decontamination factors could be calculated at the end of the tests. Five separate samples were exposed at room temperature (20°C) to five different decontamination solutions contained in glass beakers, with one sample and one solution per beaker. The compositions of the five solutions were as follows:

- Solution 1--deionized (DI) water
- Solution 2--borated water containing 2500-ppm boron as H_3BO_3, pH-adjusted to 7.5 with NaOH and 1% TRITON X-100 surfactant

- Solution 3--a solution of 5.0-wt% Na_2CO_3 and 1-wt% H_2O_2

- A two-step, alkaline permanganate and citric/oxalic acid decontamination solution consisting of

  - Solution 4A--10% NaOH and 3% $KMnO_4$

  - Solution 4B--HO_2C-CO_2H (25 g/L) and dibasic ammonium citrate (50 g/L)

- Solution 5--solution of 10-wt% HNO_3 and 0.1M HF.

One sample was placed in 50 mL of each decontamination solution, and the initial time was recorded. Beginning with 5-min intervals, 100-μL aliquots were transferred from the decontamination solutions to counting vials. To ensure representative aliquots were obtained, the decontamination solutions were mechanically stirred just before sampling, then left undisturbed until the next aliquot was taken. The vials then were gamma-ray counted in an energy- and efficiency-calibrated geometry to determine the specific activity of the Cs-137 present. A total solution activity then was calculated and plotted as a function of exposure time for each of the five decontamination solutions. As the rate of activity removal slowed, the sampling intervals were lengthened, until a total of 6 h had elapsed. At the end of 24 h, the solutions were sampled again to determine whether any unexpected chemical activity had occurred during the 18 h since the previous aliquot had been taken. Finally, the samples were removed from the solutions, rinsed with distilled water, and gamma-ray counted a second time to determine the decontamination factors.

The results of the decontamination tests, plotted as total solution activity versus time, are shown in Figure 6. Solutions 1, 2, and 3 removed a very small amount of the total Cs-137 activity, with the reaction essentially complete after about 5 h. The aliquots taken and counted after 24 h showed no significant increase in activity after the 18-h period.

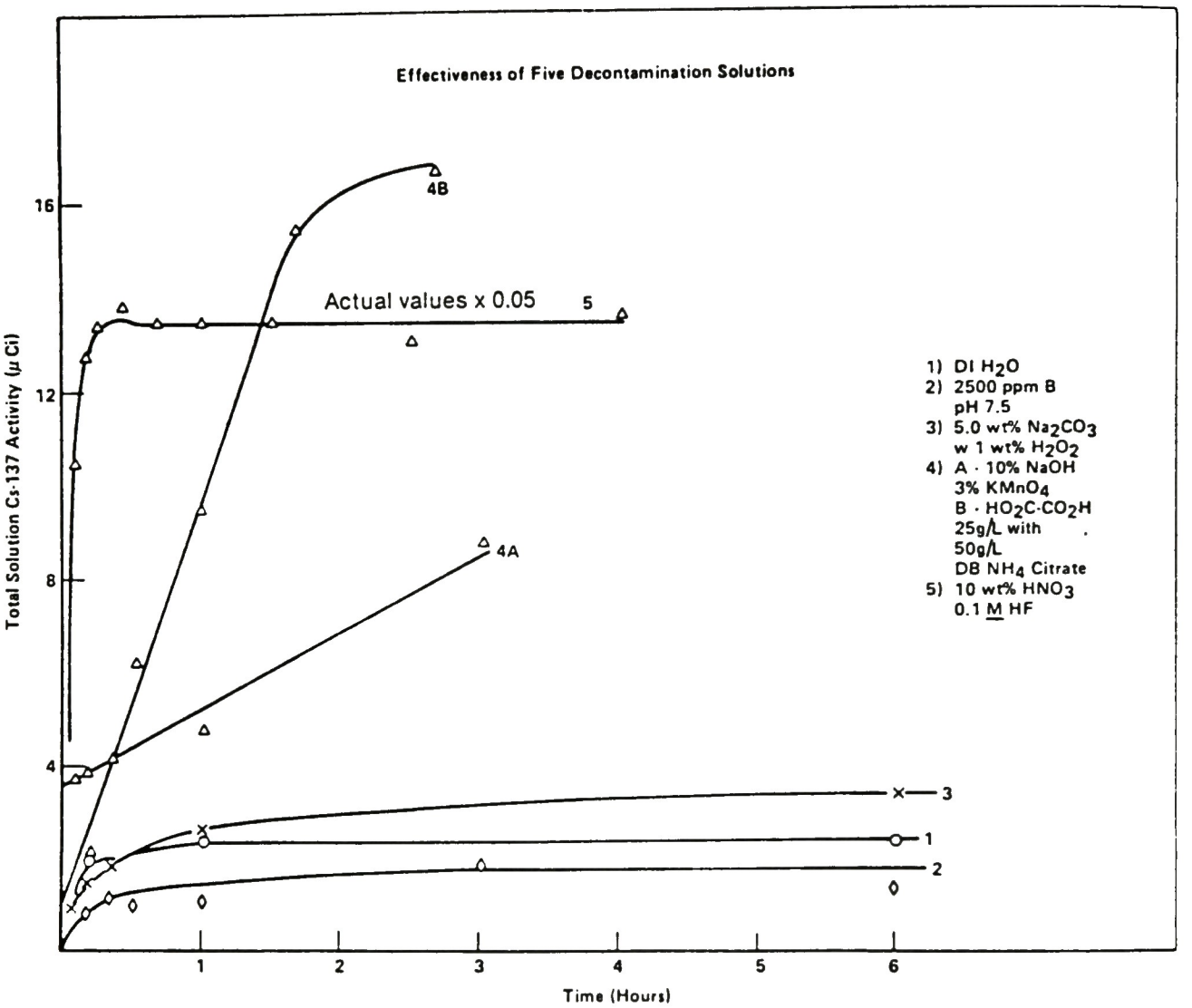

Figure 6. Effectiveness of five decontamination solutions in removing surface activity from the LS1 section.

Solution 4 actually was a two-step treatment. The sample was exposed to alkaline permanganate (Solution 4A) for 3 h and then transferred to the dibasic ammonium citrate (Solution 4B). As can be seen from Curve 4A in Figure 6, the rate of activity removal with the alkaline permanganate seems to be constant, and probably continues past 3 h. When the sample was transferred to Solution 4B, the removal rate at first increased, then appeared to level off rapidly at 2 h and 40 min. [As will be seen, the same leveling-off behavior appeared during a second test.] However, when Solution 4B was sampled after 24 h, the solution activity indicated that the removal rate had increased again and continued at an average rate of approximately 0.19 μCi/min throughout the 21-h period following the previous sampling. As discussed in Section 2.3.1.2, this behavior suggested the need for further study of the effectiveness of Solutions 4A and 4B.

The effectiveness of Solution 5 was quite dramatic, as shown by Curve 5 of Figure 6. After just 5 min, 240 μCi of Cs-137 had been removed, with apparently all of the activity removed within 25 min.

During the decontamination with Solution 5, it was quite apparent that the solution was functioning by undercutting the contaminated layer and leaching the Cs-137. The outer- and inner-diameter layers flaked away from the base metal and remained mostly undissolved after the 24-h exposure period. The base metal itself began to show evidence of chemical attack after about 25 min. Attack was indicated by dulling of the cut edge surfaces, and, after 24 h, the base metal was partially dissolved and pitted.

2.3.1.2 Detailed Tests of Two-Step Decontamination Treatment. Because of the results obtained with the two-step treatment using Solutions 4A and 4B, further study with these solutions was warranted. In these studies, the actions of Solutions 4A and 4B were investigated separately, and the two-step treatment was repeated for a longer time.

Two specimens and one additional sample from the LST section were prepared and exposed to Solution 4A alone (alkaline permanganate; Solution 4B alone (oxalic acid with dibasic ammonium citrate); and a combination of Solutions 4A and 4B, repeating the two-step treatment. The results are illustrated graphically in Figures 7, 8 and 9. Figure 7 shows that Solution 4A alone reacted with the surface layers, but its action began to level off at about 10 h. Solution 4B was more effective in removing the surface layers, as shown by the greater activity shown in Figure 8. These observations were corroborated by the calculated decontamination factors at the conclusion of the tests. The reaction, in this case, was essentially complete after about 12 h. The two-step treatment (Figure 9) was the most effective of the three treatments and showed an interesting behavior over time. After exposure to the alkaline permanganate for 3 h, followed by about 2 h in the oxalic acid solution, the reaction began to slow; the slower removal of activity also was observed in the first series of decontamination tests illustrated in Figure 6. However, in the fourth hour there was a dramatic increase in the removal of activity, which rapidly leveled off and thereafter remained essentially constant. As will be seen from the decontamination factor, about 90% of the activity was removed after exposure to Solution 4A/4B for a total of 23 h.

2.3.1.3 Calculation of Decontamination Factors. After the decontamination experiments, decontamination factors (DFs) were calculated for the solutions. The DF is the ratio of the initial activity counted for the sample/specimen to the final activity. Table 1 lists the decontamination solutions, LST sample/specimen identifications, and calculated DFs. Solutions 1 (deionized H_2O), 2 (boric acid), and 3 (Na_2CO_3-H_2O_2) had very little effect in removing the Cs-137 activity, evidenced by DFs of 1. Solution 4A alone is also relatively ineffective, with a DF of 1.1. Solution 4B alone is more effective; its DF of 6.5 indicates 85% activity removal. When Solutions 4A and 4B were used together, nearly 90% of the activity was removed. The most effective--and the most chemically aggressive--solution was the HNO_3-HF solution, which removed 100% of the activity during a 25-min exposure. However, this solution also noticeably dissolved the base metal in the same time period.

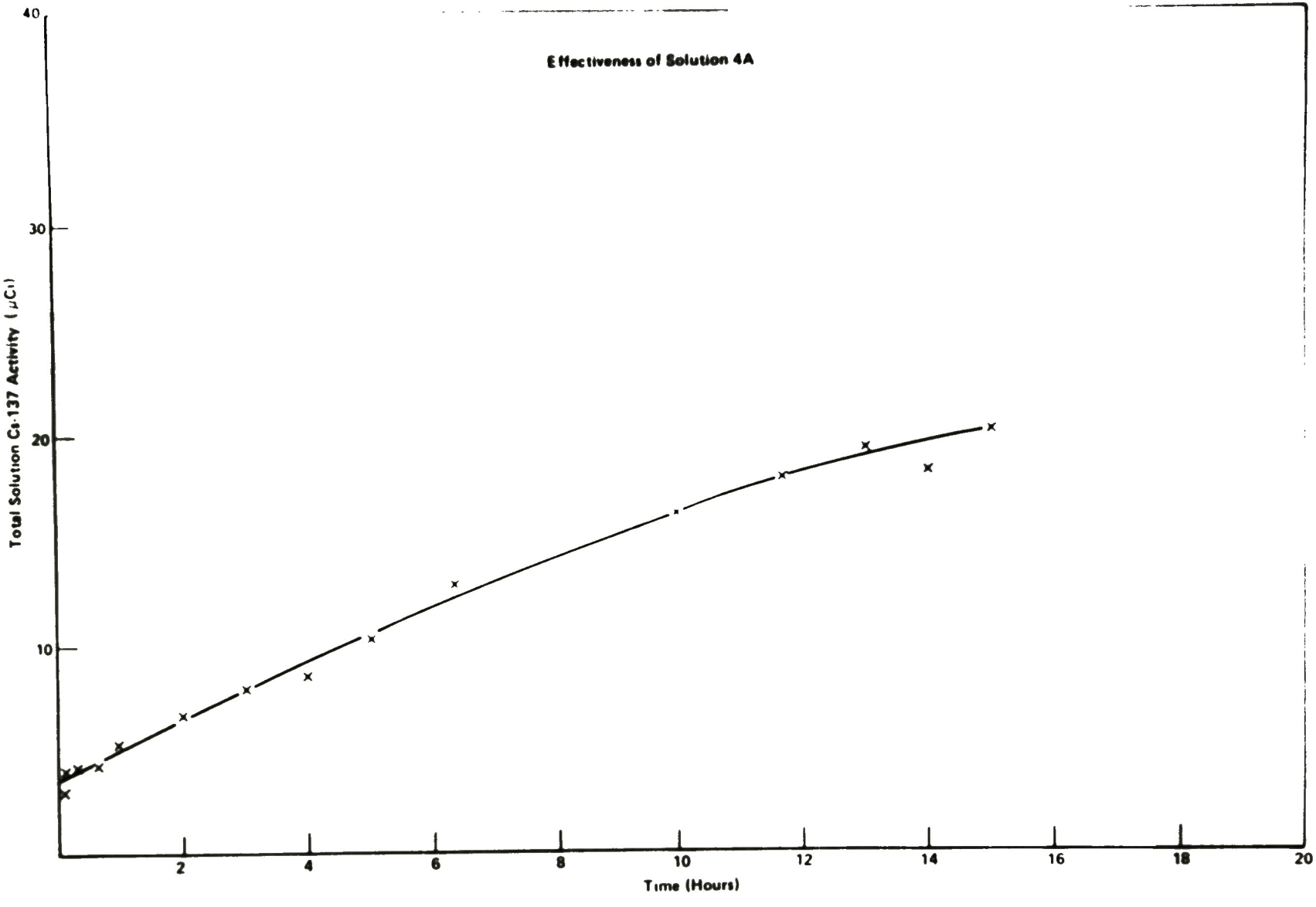

Figure 7. Decontamination effectiveness of an alkaline permanganate solution (Solution 4A).

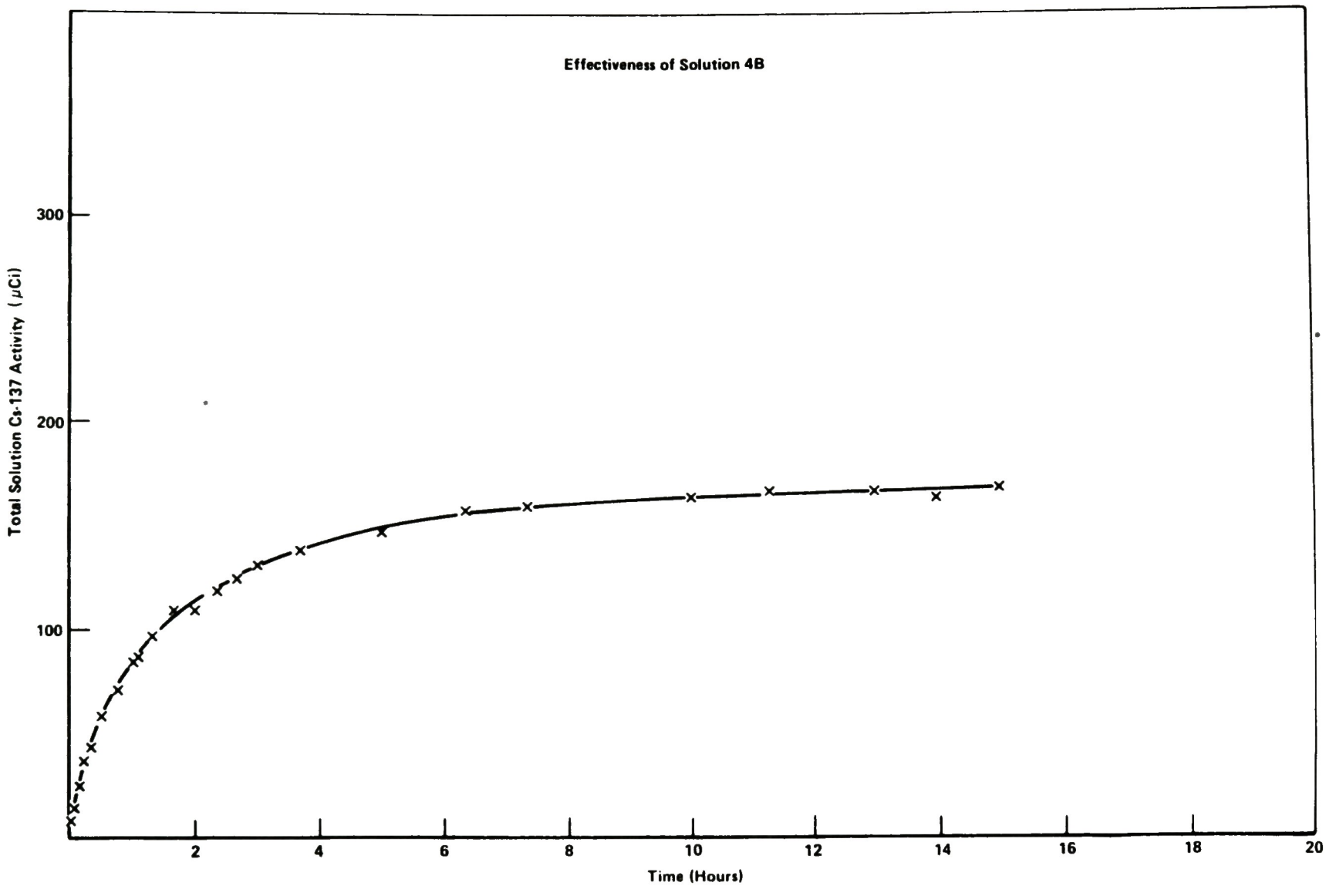

Figure 8. Decontamination effectiveness of an oxalic acid/dibasic ammonium citrate solution (Solution 4B).

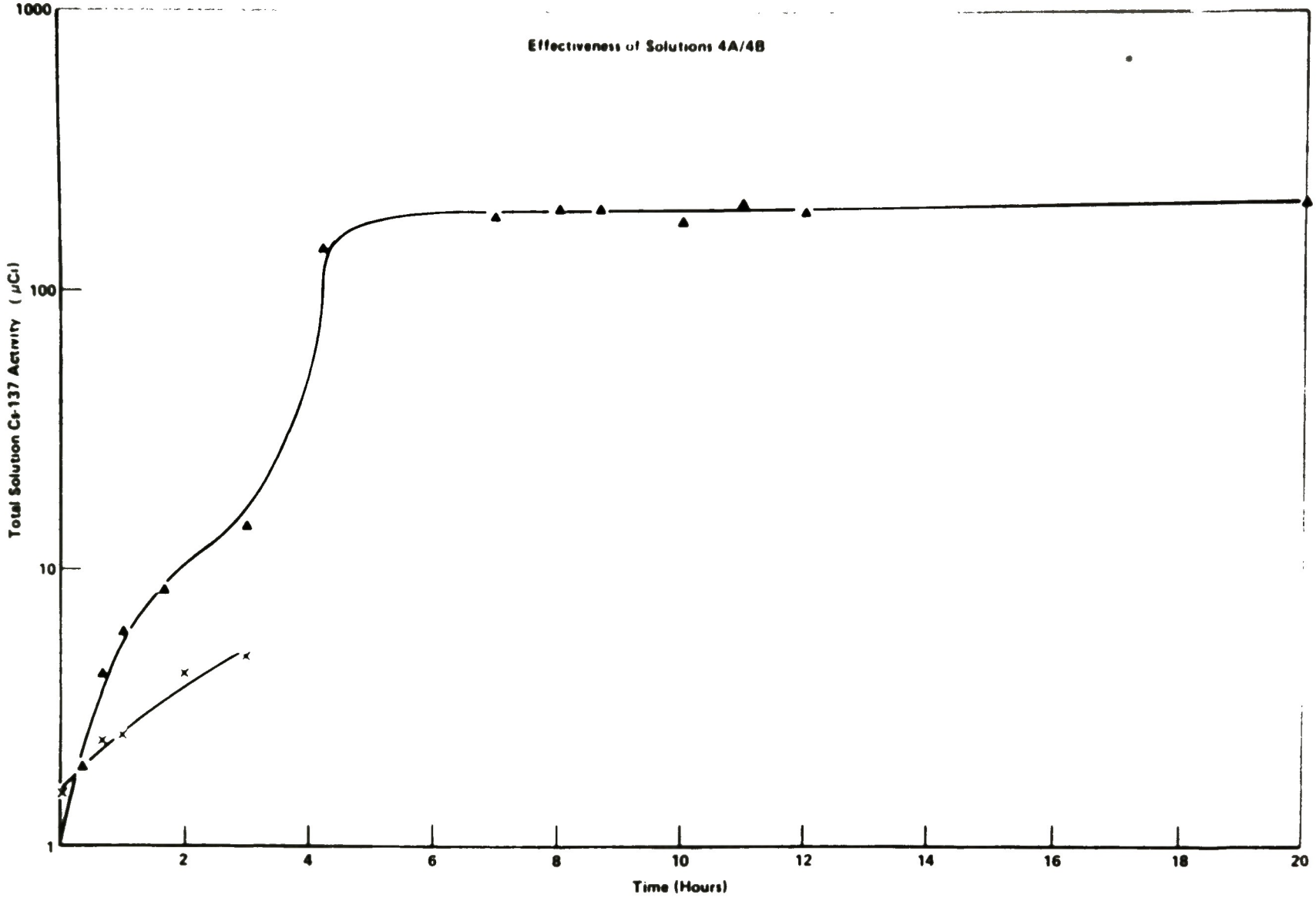

Figure 9. Decontamination effectiveness of two-step treatment, using an alkaline permanganate solution (Solution 4A) and an oxalic acid/dibasic ammonium citrate solution (Solution 4B).

TABLE 1. EFFECTIVENESS OF THE DECONTAMINATION SOLUTIONS IN REMOVING SURFACE CS-137 ACTIVITY

Test	Solution	Sample/Specimen	Decontamination Factor[a]
Initial tests	1	4-3.1	1
	2	4-3.2	1
	3	4-3.3	1
	4A/4B	4-3.4	8.8
	5	4-2.1	∝
Tests of two-step treatment	4A	6-1	1.1
	4B	6-2	6.5
	4A/4B	4-2.2	8.9

a. Defined as the ratio of the initial activity to the final activity.

2.3.2 Separation, Collection, and Dissolution of the Surface Layers

Work conducted by Babcock and Wilcox (B&W) on a section of leadscrew indicated the presence of two layers of deposited material, in addition to the normal in-service oxide layer.[2] The two layers were referred to as the loosely adherent deposit (LAD) and the tightly adherent deposit (AD). They were separated at B&W by a qualitative brushing procedure; the material that could be removed by vigorous brushing with a stainless steel brush constituted LAD, and the remaining material was AD. As will be discussed in later sections, two layers also were observed on the LST section examined by Battelle Columbus Laboratories. The appearance and the boundary of the two layers were better defined on the outer surface than on the inner surface. A brushing technique similar to that used by B&W was used to separate the LAD from the AD on both the outer and inner surfaces of the LST section.

Ring 6 was used for the separation and collection of LAD and AD. The ring was transferred to a glove box and cut into halves. Next, metal shavings were removed from the edges of the cut halves, and the halves were transferred to clean polyethylene bags so metal fines and other possible contaminants could be removed from the glove box.

In the glove box, one of the halves of Ring 6 was removed from the polyethylene bag. Attempts were made to collect deposits, first by brushing with a bristle brush and then by scraping with a nickel spatula. Neither method removed the deposits, except for a few, barely visible particles. Next, the outer surface was brushed with a stainless steel brush. This method did remove some surface material, which was collected on a paper sheet and transferred to a glass vial. Brushing was continued until all the LAD was removed. The outer surface of the other half of Ring 6 then was brushed in a similar manner. The material collected from the outer surfaces was designated as OD-LAD.

Next, the inner surfaces of the two halves were brushed gently with a fine bristle brush to remove any OD-LAD, which could mask chemical and

radiochemical differences between the outer and inner surfaces. The inner surfaces of the two halves then were brushed vigorously with a second, contamination-free, steel brush. The removed material was collected and placed in a glass vial. The material collected from the inner surfaces was designated as ID-LAD.

Two small samples from each half of Ring 6 were obtained for subsequent analysis. After the subsectioning and transfer of the samples, the glove box was cleaned once again to remove metal fines which could contaminate the AD samples.

The OD-AD was removed by carefully filing the outer surfaces of each half-ring with a triangular metal file until the base metal became just visible. The material was collected on paper and transferred to a glass vial. The ID-AD was removed using a rounded file, while collecting the material on paper. Removing the ID-AD and minimizing the introduction of base metal was more difficult because of the shape of the surface. The ID-AD near the middle of the ring halves could not be filed off without introducing base metal shavings. Consequently, the material was left on the middles of the half-rings. Generally, the process seemed to work quite well, with no metal fragments visible in any of the collected material. The collected material was labeled (OD-LAD, ID-LAD, OD-AD, and ID-AD) and transferred to a radiochemistry laboratory for further analysis.

To perform radiochemical and chemical analyses of the LAD and AD layers, it was necessary to dissolve the material. Initially, it was planned to use HNO_3-HF to dissolve the material for some of the analyses. However, the decontamination tests showed that very little of the surface material dissolved in this mixture. An attempt then was made to digest the material via Na_2CO_3 fusion. This also was ineffective, digesting virtually none of the material. Subsequently, the fusion medium was changed to a strongly acidic and oxidizing potassium pyrosulfate ($K_2S_2O_7$) fusion. This was successful.

Small amounts of the LAD and AD material, ranging in weight from 5.1 to 27.6 mg, were mixed with 1 g of $K_2S_2O_7$ in a porcelain crucible. The crucible was heated gently over a Fisher burner until the $K_2S_2O_7$ melted and began to decompose and produce sulfur trioxide (SO_3). Digestion of the LAD or AD was almost immediate after evolution of SO_3 began, and the entire LAD or AD material appeared to be digested. Then 2N H_2SO_4 was added to the cooled crucible with the melt. The melt dissolved rapidly, but the resulting solution appeared cloudy, indicating undissolved colloidal material. Gentle heating for about 10 min at 90°C produced clear solutions, with no evidence of undissolved material. The digested and dissolved LAD and AD material was diluted with 2N H_2SO_4 to a known volume and transferred to polyethylene bottles for subsequent chemical and radiochemical analysis.

2.3.3 Elemental Analysis of Loosely Adherent and Adherent Deposits

Material from the outer diameter (OD) and inner diameter (ID) of the LST was analyzed by (a) inductively coupled argon plasma (ICAP) spectroscopy for elemental analysis, (b) x-ray diffraction (XRD) for compound identification, (c) electron spectroscopy for chemical analysis (ESCA) for compound identification, and (d) secondary ion mass spectrometry (SIMS) for a depth profile through the corrosion layer.

2.3.3.1 ICAP Analysis. The surface deposit materials discussed in Section 2.3.2 were analyzed by ICAP spectroscopy for the elements B, Na, Mg, Al, Si, Ca, Ti, V, Cr, Mn, Fe, Co, Ni, Cu, Zn, Zr, Mo, Ag, Cd, In, Sn, Pb, and U. In addition, cesium was determined by atomic absorption, which is more sensitive than ICAP for this element. The results are listed in Table 2.

The results show that the control rod material containing Ag, In, and Cd is associated primarily with the OD deposits. The high iron and nickel contents (60 and 11%, respectively) in the ID-AD indicate that a significant amount of base metal probably was removed during the filing operation, although this was not evident from visual inspection of the

TABLE 2. ELEMENTAL ANALYSIS OF THE SURFACE DEPOSITS DETERMINED VIA ICAP SPECTROSCOPY

Element	Concentration (%)			
	ID-LAD	OD-LAD	ID-AD	OD-AD
B	<0.1	<0.08	<0.04	<0.02
Na	3.1	0.79	0.60	0.72
Mg	<0.5	<0.5	<0.2	<0.1
Al	<0.5	<0.5	<0.2	<0.1
Si	0.47	<0.2	0.73	2.8
Ca	<0.2	<0.2	<0.07	0.1
Ti	<0.05	<0.05	<0.01	<0.01
V	<0.1	<0.1	<0.02	<0.02
Cr	7.1	5.6	19.	9.1
Mn	0.8	0.5	1.4	0.6
Fe	41.	22.	60.	23.
Co	<0.05	<0.05	<0.02	<0.01
Ni	4.3	3.3	11.	5.4
Cu	<0.1	<0.1	<0.04	<0.02
Zn	<0.1	<0.1	<0.04	<0.02
Zr	~0.6	~0.4	<0.2	<0.09
Mo	<0.1	<0.1	0.38	<0.09
Ag	4.0	32.	<0.3	1.1
Cd	0.4	0.5	<0.3	<0.2
In	1.1	4.3	~0.3	<0.2
Sn	0.57	2.8	<0.2	0.23
Cs	<19	<16	<6.6	<3.6
Pb	<0.5	<0.5	<0.2	<0.1
U	--	--	--	--
Total	60.3	71.4	92.8	42.4

collected material. The high upper limit for cesium (in the percent range) reflects the poor sensitivity of atomic absorption for this element. The uranium could not be determined, due to interference of an unknown nature.

2.3.3.2 XRD Analyses. Results of the XRD analysis of OD-AD and ID-AD material from the LST section are given in Table 3. The disordered taenite phase is probably from Inconel alloys in the sample. This material has a face-centered cubic structure, with Fe and Ni occupying random lattice sites; hence the "disordered" designation. The line due to silver was observed only in the OD-AD material. The lack of any silver line in the ID-AD also is supported by ESCA and ICAP findings, which detected no silver in the layer.

2.3.3.3 ESCA. Specimens for analysis were obtained from the inner and outer surfaces of the LST section. Table 4 lists the results for Specimen 4-6 which was an OD surface specimen with both layers intact. Table 5 lists measured values for Specimen 6-4, another OD surface specimen with the LAD removed. The values shown in Table 6 are for Specimen 4-5, an ID surface specimen with both layers intact. The depth profile data were obtained from successive analyses after argon ion sputtering had removed overlying material. The specimen surfaces were analyzed in the Leybold Heraeus LHS-10 system. ESCA utilizes the characteristic x-ray photons from a magnesium anode to ionize electrons from the specimen. The binding energies are characteristic quantities for a certain shell of the element. If the elements contained in a specimen present themselves as chemical compounds, the binding energies of the electrons of the compound components will be slightly different from those belonging to the atomic state. This is called the chemical shift, which normally amounts to a few tenths of an electron volt up to several electron volts.

Each specimen was analyzed, using low-resolution scans for quantification and high-resolution scans for each element to define the binding energies accurately. The binding energies were compared to literature values or reference values to determine compound components. The analyses were quantified by using the area under the peak times the

TABLE 3. RESULTS OF XRD ANALYSIS OF THE ADHERENT DEPOSITS

Deposit Layer	Compound	Powder Diffraction File	Relative Pattern Strength
OD-AD	γ-Fe, Ni (disordered taenite)	23-297	Very strong
	Fe_3O_4 (magnetite)	19-629	Medium
	α-Fe (iron)	6-696	Weak
	Ag (silver)	4-783	Very weak
	Unknown (1.34 Å)		Very, very weak
ID-AD	γ-Fe, Ni (disordered taenite)	23-297	Very strong
	Fe_3O_4 (magnetite)	19-629	Weak
	α-Fe (iron)	6-696	Very weak

TABLE 4. ESCA DATA FOR SPECIMEN 4-6 OD
(both layers intact)

Depth (Å)	Relative Concentration[a] (at.%)											
	Fe	Ni	Cr	O	In	Cd	Ag	C	Cs	B	Te	Sn
0	0.2	-	--	29.9	0.5	0.7	0.4	64.2		4.1	--	-
100	1.7	-	--	30.1	0.7	1.0	0.6	60.6	--	5.3	-	-
250	4.5	-	--	25.2	0.7	0.5	0.9	61.5	--	6.6	--	-
500	3.1	-	--	31.5	0.9	0.4	1.0	57.9	--	5.2	--	-
1000	10.4		--	39.9	0.8	0.8	1.3	41.0	-	5.8	--	-
2000	11.8	Trace[b]	Trace	51.8	1.3	0.7	1.6	24.7	Trace	8.2	Trace	-

a. Iodine was not detectable with a detection limit of <0.05 at%.

b. Trace indicates <0.05 at.%.

TABLE 5. ESCA DATA FOR SPECIMEN 6-4 OD
(LAD removed)

Depth (Å)	Relative Concentration[a] (at.%)								
	Fe	Ni	Cr	O	C	Cd	Te	In	Ag
0	4.4	0.7	1.7	28.9	61.2	1.8	1.1	0.2	Trace[a]
250	4.4	0.7	1.7	31.4	59.3	1.7	0.7	0.2	Trace
500	5.0	0.7	2.5	33.6	55.1	1.6	1.0	0.3	--
1000	5.2	1.2	3.8	44.2	43.2	1.5	0.8	Trace	--
2000	5.5	1.1	3.1	55.0	32.0	2.0	1.3	-	--

a. Trace indicates <0.05 at.%.

TABLE 6. ESCA DATA FOR SPECIMEN 4-5 ID
(both layers intact)

Depth (Å)	Relative Concentration (at.%)				
	Fe	Ni	Cr	O	C
0	1.7	0.3	0.7	20.0	77.3
100	7.4	1.3	2.8	36.8	51.6
250	9.0	1.4	4.7	45.8	39.0
500	8.8	1.4	5.9	45.4	38.5
1000	9.0	1.5	5.9	46.7	36.9
2000	9.1	1.5	6.1	47.0	36.3

elemental sensitivity. ESCA is an average analysis over a circular area of 1 cm^2 and a depth of 30 Å, which represents the limit for electron escape from a solid specimen. For the high resolution scans, literature values of the binding energies indicated that B, Fe, In, Cd, and Ag were present in oxide form as BO, Fe_3O_4, InO, CdO, and AgO. Nickel and chromium oxides (NiO and Cr_2O_3) may be present, but below detection limits.

2.3.3.4 SIMS Analysis. The OD surface of Specimen 4-6, with both layers intact, was analyzed by SIMS to determine the depth profile of the corrosion layer. SIMS is particularly sensitive to the light elements in the ppm range.

The SIMS apparatus is a modified Cameca IMS 300. In operation, a primary beam of ions or neutral atoms is directed onto the surface under study. Secondary ions, resulting from the collision between the primary beam and the surface, are ejected from the surface and detected. Analysis of the secondary ions indicates the surface composition. The change in concentration as a function of depth can be obtained by gradually removing material by sputtering with the primary beam.

In normal operation, a primary beam of positive ions impinges upon a surface. Secondary ions released by sputtering are energy-filtered and mass-analyzed. The unique stigmatic focusing of the IMS 300 permits two types of data acquisition: an ion image of the surface or an analog signal of mass intensity. Spatial resolution of about 1 μm is attainable, while depth resolution of 50 Å is attained routinely.

The machine operates under computer control by a PDP 11-34 and can operate in either continuous scan mode or depth-profiling mode, in which up to ten separate chemical species can be monitored.

Table 7 lists the instrument intensities for the elements detected. For a given instrument intensity, the magnitude of response of each element is different; consequently, the instrument intensities of different elements do not indicate relative elemental concentration. However, for

TABLE 7. INSTRUMENT INTENSITIES FOR ELEMENTS DETECTED BY SIMS ANALYSIS OF SPECIMEN 4-6 OD
(both layers intact)

		Scan					
Element	Mass	1	2	4	6	8	10
B	11	430	380	200	200	100	100
Na	23	4,300	3,600	3,400	3,400	3,200	3,200
Al	27	6,400	6,900	3,900	2,800	2,600	2,200
Si	28	580	500	450	450	400	400
Ca	40	520	300	200	170	150	130
Cr	52	99,000	131,000	131,000	131,000	131,000	131,000
Fe	56	12,000	113,000	110,000	101,000	90,000	85,000
Zr	90	150	170	170	200	200	200
Ni	58	1,420	2,600	4,800	6,000	6,400	6,400
CrO	68	2,100	3,600	3,800	4,200	4,400	4,400
FeO	72	1,500	1,500	1,500	1,300	1,100	1,100
Ag	107	1,900	1,500	1,600	1,700	1,400	1,200
Cd	113	1,100	800	720	670	650	650
In	115	19,700	10,400	9,800	9,600	9,200	9,400
Te	130	90	100	80	80	90	90
Sn	120	200	200	100	120	120	100
Cs	137	200	200	300	400	500	500
I	129	200	140	140	120	120	120
U	238	300	300	240	200	200	180

each individual element, the indicated instrument intensities are proportional to the concentration of that element. The total depth achieved during the analysis was about 3 μm.

2.3.3.5 Conclusions from Elemental Analyses. The presence of many elements other than Fe, Cr, and Ni indicate there was considerable mobility of core materials. The Ag, In, and Cd must have been transported as metals, with surface oxidation taking place after deposition. This is suggested by the metallic globules embedded in the surface deposit. The presence of Cs, I, and U also indicates the mobility of core materials.

2.3.4 Specific Activity Measurements of the Gamma-Ray-Emitting Radionuclides

The digested and dissolved LAD and AD material was used to determine specific activities of the gamma-ray-emitting radionuclides. A 100-μL aliquot of solution from the digestion (see Section 2.3.2) was counted in an energy- and efficiency-calibrated geometry of the previously described high purity germanium detector system (see Section 2.1.2) The only gamma-ray-emitting radionuclides observed were Cs-134 and Cs-137. Table 8 lists the measured specific activities of both radioisotopes for the LAD and AD material, as well as the calculated ratios of the two activities.

The OD-LAD appears to have about 17% more activity per unit mass than the ID-LAD. The difference in activity per unit mass between the OD-AD and ID-AD is much more dramatic, with OD-AD activity 8.4 times greater than that of the ID-AD.

The activity per unit area for the AD on both the OD and ID surfaces was measured. This was done inside a glove box by removing the deposits from small, scraped specimens of the LST section, with a file. The surface to be measured also was filed until the remaining area of surface deposit was small enough to be gamma-ray counted directly. The samples then were rinsed with hexane to remove loose surface contamination. The results of the measurements are listed in Table 9. Again, only Cs-134 and Cs-137 were observed.

TABLE 8. SPECIFIC ACTIVITY MEASUREMENTS OF THE LAD AND AD LAYERS

Deposit Layer	Nuclide	Specific Activity Bq/mg	Specific Activity µCi/g	Ratio Cs-137/Cs-134
OD-LAD	Cs-137	4.31×10^5	1.17×10^4	
	Cs-134	2.00×10^4	5.39×10^2	21.7
ID-LAD	Cs-137	3.70×10^5	1.00×10^4	
	Cs-134	1.55×10^4	4.18×10^2	23.9
OD-AD	Cs-137	2.43×10^6	6.57×10^4	
	Cs-134	1.05×10^5	2.82×10^3	23.3
ID-AD	Cs-137	2.89×10^5	7.81×10^3	
	Cs-134	1.29×10^4	3.49×10^2	22.4

TABLE 9. SURFACE ACTIVITY MEASUREMENTS OF THE OD AND ID ADHERENT DEPOSIT LAYERS

Sample	Nuclide	Surface Activity Bq/cm^2	Surface Activity µCi/cm^2	Ratio Cs-137/Cs-134
6-1.1 OD	Cs-137	4.62×10^7	1250	
	Cs-134	2.01×10^6	53.1	23.5
6-1.2 ID	Cs-137	2.35×10^7	633	
	Cs-134	9.91×10^5	26.8	23.4

Detection limits for other, less abundant gamma-ray emitters were calculated based on actual LST gamma-ray spectra and the methods described by Currie.[3] For Ru-106 and Sb-125, detection limits were less than about 0.2% of the measured Cs-137 activity; and for Mn-54, Co-60, and Ag-110m, less than about 0.02% of the activity of Cs-137. None of the radionuclides were detected. The surface activity of the ID-AD was found to be about half the OD-AD activity.

2.3.5 Strontium-90 Analysis of LST Deposits

Both LAD and AD material from the LST section were collected, dissolved, and analyzed for Sr-90. Because of the lack of any gamma ray of significant abundance associated with the decay of Sr-90 or its daughter Y-90, Sr-90 analysis must be accomplished using counting techniques sensitive to beta particles. Because of the counting technique, it is essential that separation of Sr-90 relative to all other beta emitters be maximized. Thus chemical methods are required to separate Sr-90 from its daughter Y-90 and from Cs-134 and Cs-137, major components of the deposits.

Each of the four deposits, designated ID-LAD, OD-LAD, ID-AD, and OD-AD, was dissolved by fusion with potassium pyrosulfate (see Section 2.3.2). Portions of the solutions were used for the Sr-90 analyses.

2.3.5.1 Sr-90 Separation. Figure 10 is a flow chart showing the steps involved in separating Sr-90 from the other radionuclides. In each case, a known quantity of inactive strontium carrier was added to aid separation. After separation and washing, the strontium carbonate ($SrCO_3$) precipitate was dissolved in a few drops of 6M HNO_3, transferred quantitatively to a 10-mL volumetric flask, and diluted to the mark with distilled water. A 500-µL portion of this solution was extracted using an Eppendorf pipette and diluted to 100 mL in a volumetric flask with 0.1M HCl. The 100-mL solutions were analyzed later for strontium by atomic absorption, in order to derive yield estimates.

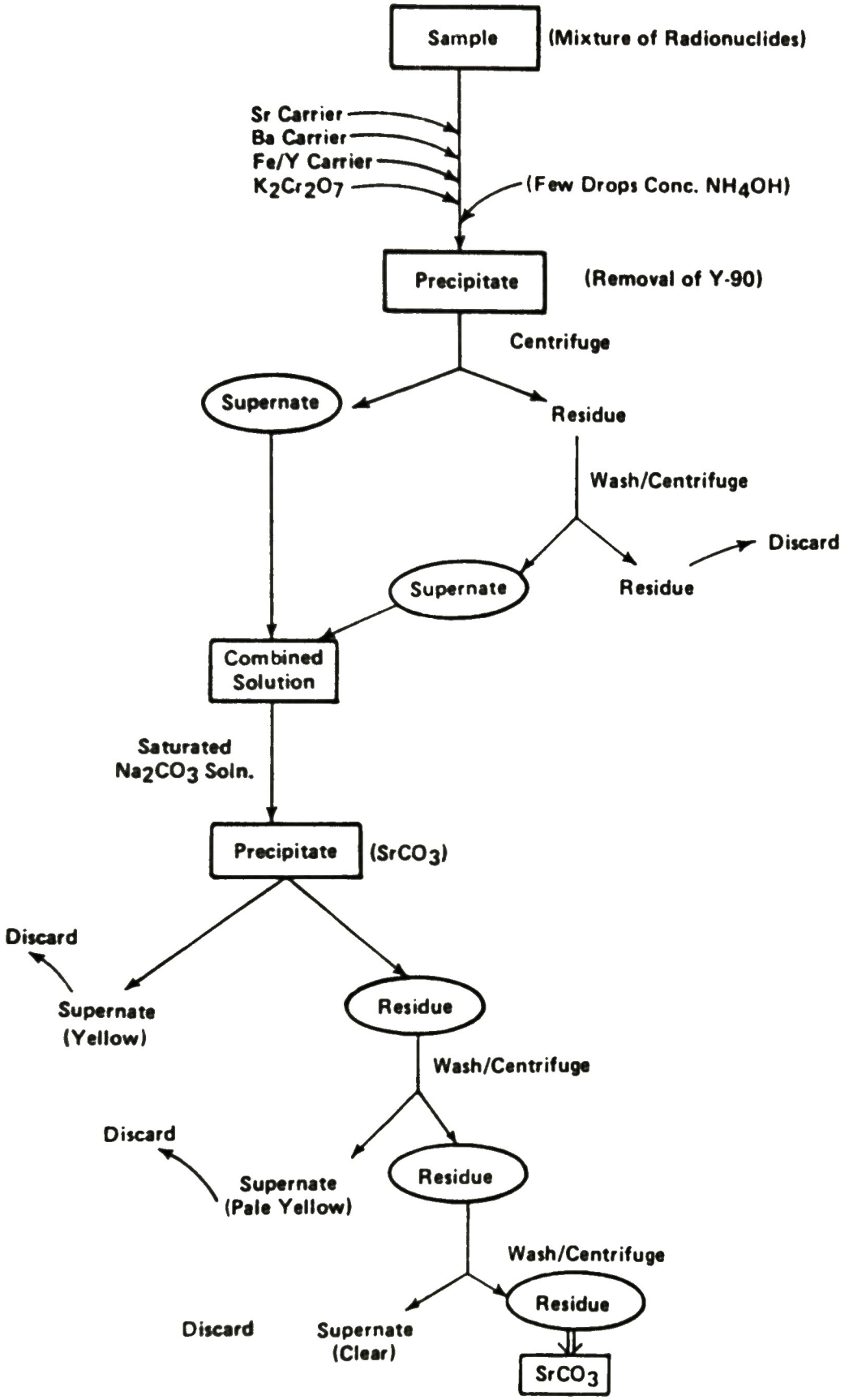

Figure 10. Flow chart showing steps involved in separating Sr-90 for analysis.

The remainder (9.5 mL) of each solution was transferred quantitatively to a 25-mL plastic vial to which 10 mL of scintillation cocktail (Insta Fluor) was added. The mixture was shaken to form a stable gel. The complete Sr-90 analysis was performed at least in duplicate. For blank standards, the same chemical procedure was applied to distilled water. Each solution was counted as soon as possible after preparation, for a minimum of 10,000 counts. In addition, solutions were recounted on at least two occasions to obtain data relating to the growth of the daughter nuclide, Y-90. For detection efficiency, a Sr-90 standard was prepared by mixing 1 mL of a standardized Sr-90/Y-90 solution with 9 mL of distilled water plus 10 mL of scintillation cocktail.

An efficiency calibrated Searle Analytic, Inc. Liquid Scintillation Counter, Model 6880, was used to measure Sr-90 activities. This machine features automatic, energy-window settings and corrects automatically for quenching. [Quenching is a slight reduction in counting efficiency resulting from the presence of impurities.] Besides presenting raw data, the printout provides net activities in counts per minute and information on the presence of impurities by means of a quench factor. In all cases, this quench factor (the ratio of count rates appearing in internally-programmed energy windows) was similar and could thus be ignored as a significant variable.

2.3.5.2 Results and Discussion of Sr-90 Analyses. Triplicate analysis of the AD and duplicate analyses of the LAD were performed using the separation scheme flow-charted in Figure 10. For calculating Sr-90 activities from the data provided by liquid scintillation counting of the solutions, the contribution to the total activity from Y-90, the daughter nuclide of Sr-90, must be determined. This can be calculated using the following equation:

$$A_{Y\text{-}90} \text{ at counting time} = A_{Sr\text{-}90}\,[1 - e^{-(0.693t/t_{1/2})}] \qquad (1)$$

where

$A_{Y\text{-}90}$ = activity of Y-90 in the solution

$A_{Sr\text{-}90}$ = activity of Sr-90 in the solution

$t_{1/2}$ = half-life of Y-90 (64.1 h)

t = time elapsed since chemical separation of Y-90 from Sr-90.

Knowing both the chemical separation and counting times, $A_{Y\text{-}90}$ was calculated for each sample and for each counting period.

The averaged results are expressed in activity per unit weight in Table 10. The overall analytical uncertainty of the Sr-90 method, including dissolution, chemical yield analysis, and radioactivity measurement, is estimated to be no greater than 20% and is included as the error expressed in Table 10. Also given in the table are values of Sr-90 activity per unit area for the LAD. The values were obtained by estimating the areas of the LST from which the deposits were obtained. Since all of the LAD material from each surface was dissolved, it was possible to relate the Sr-90 activity to surface area. For the AD solutions, an unknown fraction of the material removed from the surfaces was used to prepare the AD solution. Therefore, it is not possible to directly relate the Sr-90 measurements to the surface activity for the AD deposits.

2.4 Metallographic Analysis

2.4.1 Metallography and SEM Examination of Deposits

Specimens from the LST section were examined by metallography and scanning electron microscopy to characterize the microstructure of the deposits. Four separate specimens, one each from Rings 1 and 2 and two

TABLE 10. SR-90 ACTIVITY OF THE LST DEPOSITS

Deposit Layer	Sr-90 Activity (μCi/g)	Sr-90 Activity ($\mu Ci/cm^2$)
OD-AD	145 ± 29	--[a]
ID-AD	6.6 ± 1.3	--[a]
ID-LAD	390 ± 78	0.2
OD-LAD	450 ± 90	0.2

a. Unknown.

from Ring 5, were examined. [Ring 1 was from the bottom of the LST section, and Ring 5 was located approximately 5 cm from the bottom end.] The specimen from Ring 1, designated as Specimen 1-1, was a longitudinal specimen. The others were transverse specimens.

2.4.1.1 Metallography. The metallographic specimens were cut from the rings dry, taking care to avoid damaging the deposits. They were mounted using a cold-setting epoxy resin. The specimens were ground and polished using silicon carbide abrasive papers and diamond paste. To prevent the loss of soluble radionuclides, nonpolar lubricants such as kerosene were used during grinding and polishing. The specimens then were rinsed with hexane.

The specimens were examined in detail using a Leitz Model mm 5 RT metallograph, and their important features were documented by photography. Significant results from this examination are as follows:

- Specimen 1-1, a longitudinal specimen, exhibited a large number of bright metallic particles (globules) at the bottom end. These particles also were present in the outer surface deposit, but in much smaller quantities. The globular appearance of the particles suggests they may have been molten at one time. Figures 11 through 13 show the appearance of the particles in this specimen.

- The deposits on all of the specimens consisted of two separate and identifiable layers--presumably the loosely adherent and the tightly adherent layers.

- The loosely adherent layer varied widely in thickness and porosity.

- There was a significant difference in the nature of the loose deposits on the inner and outer surfaces of the LST section. In the inner surface deposits, the boundaries appeared to be less well defined than in the outer surface deposits.

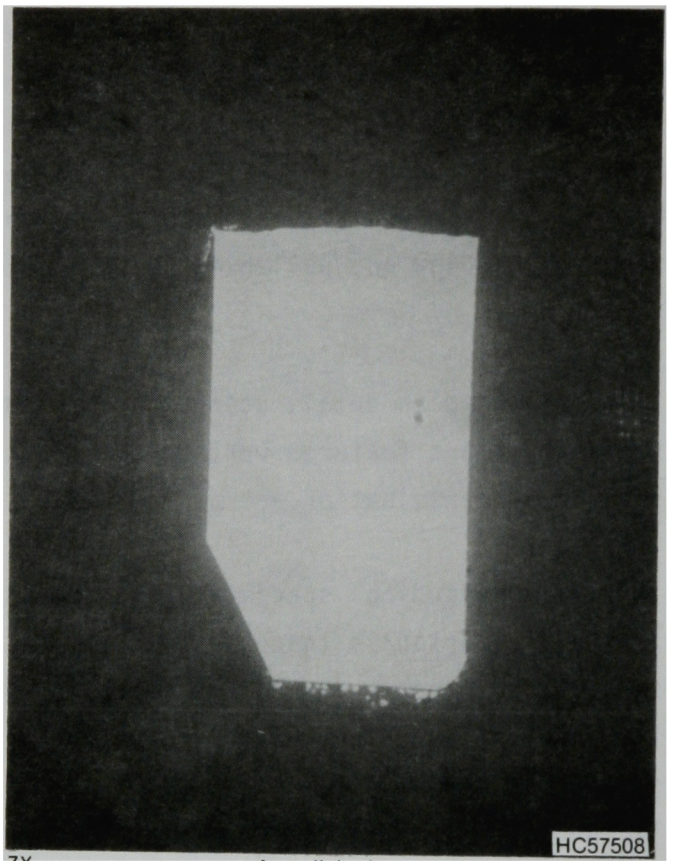

Figure 11. Photomacrograph of Specimen 1-1, showing metallic particles at the bottom end of the LST section.

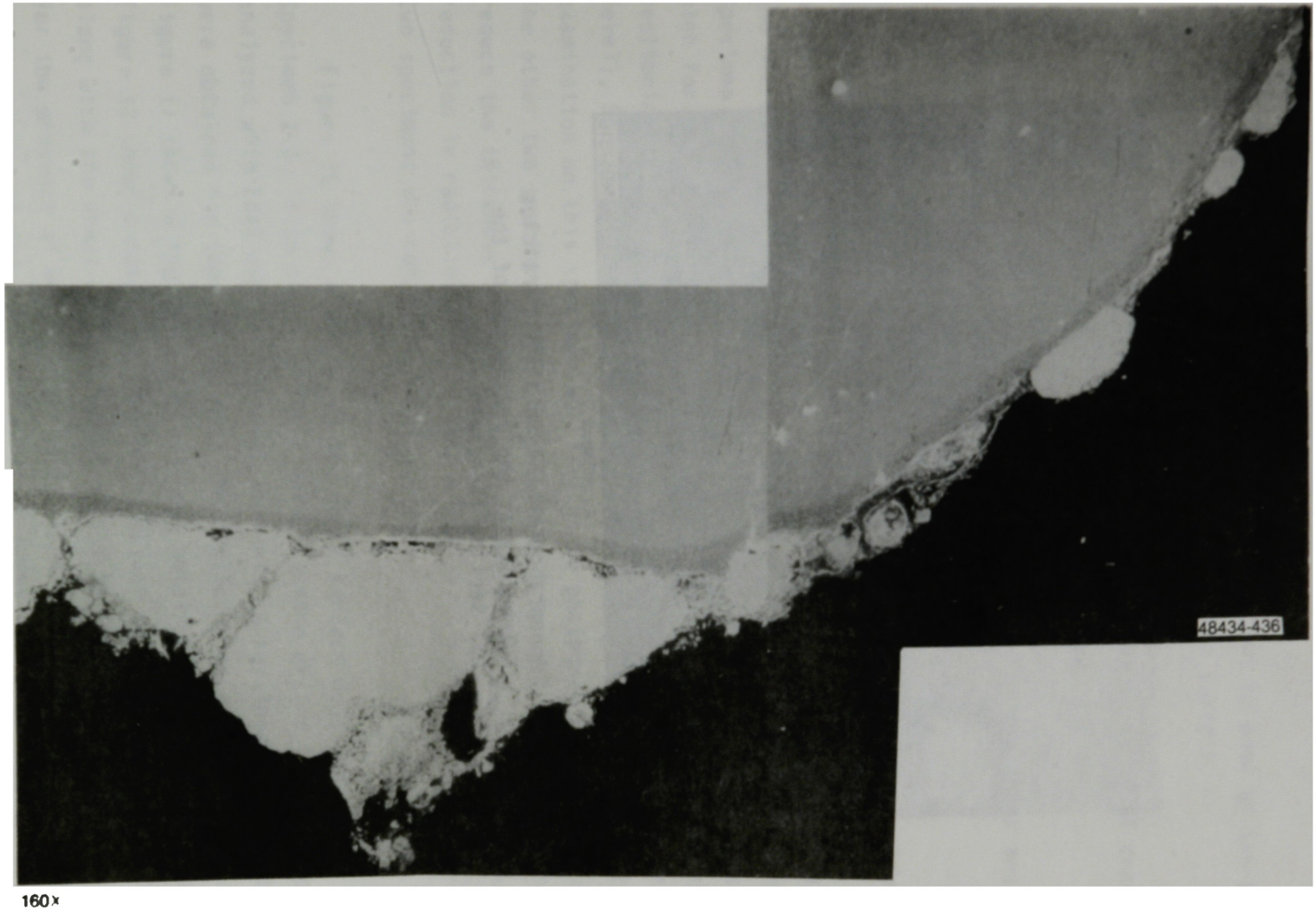

160×

Figure 12. Appearance of the bright metallic globules at the bottom end of the LS1 section (Specimen 1-1).

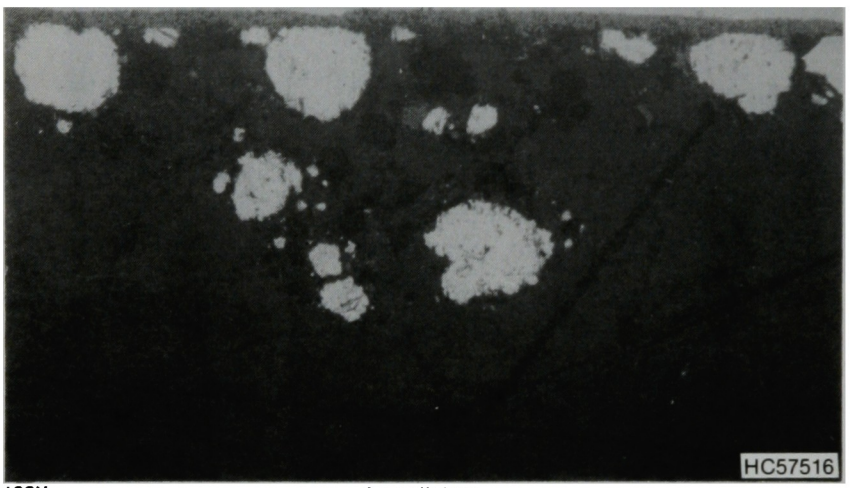

100X As polished

Figure 13. Appearance of the metallic particles (globules) at the bottom end of the LST section (Specimen 1-1).

- The adherent deposits appeared similar on the outer and inner surfaces.

- The inner surface deposits exhibited few, if any, of the bright metallic particles observed on the outer surface.

- None of the specimens examined showed any evidence of cracking or intergranular attack.

Figures 14 and 15 show the typical appearance of the inner and outer surface deposits on Specimens 1-1 and 5-6.

2.4.1.2 Scanning Electron Microscopy (SEM). Three of the four metallographic specimens were examined using the scanning electron microscope. The primary purpose of this examination was to characterize the microchemical composition of the deposits. Initial examination of Specimen 1-1 indicated that the radiation level of the specimen was too high for the use of energy dispersive x-ray analysis (EDAX). During sectioning to reduce the size of the specimen (and thus its radiation level), Specimen 1-1 separated from its mount; consequently, the scope of examination on this specimen was limited to photographic characterization. The other two specimens (Specimens 5-6 and 2-3) were sectioned further to reduce the thickness and the associated radiation level. With this reduction in radiation levels, EDAX analysis of a number of areas in the two specimens was completed successfully.

Figure 16 shows a mosaic of the outer surface deposits on Specimen 2-3. Also shown in the figure are some of the typical locations analyzed with EDAX and the elements present. X-ray intensity spectra also were obtained for some of the over 100 particles or areas analyzed. Figure 17 shows a typical x-ray spectrum obtained for a small particle. Figure 18 shows a mosaic of the inner surface deposits from Specimen 2-3, along with the areas or locations analyzed by EDAX and the results. Except for the presence of metallic particles on the outer surface, the results of EDAX analyses of the inner and outer surfaces of the LST appear to be similar.

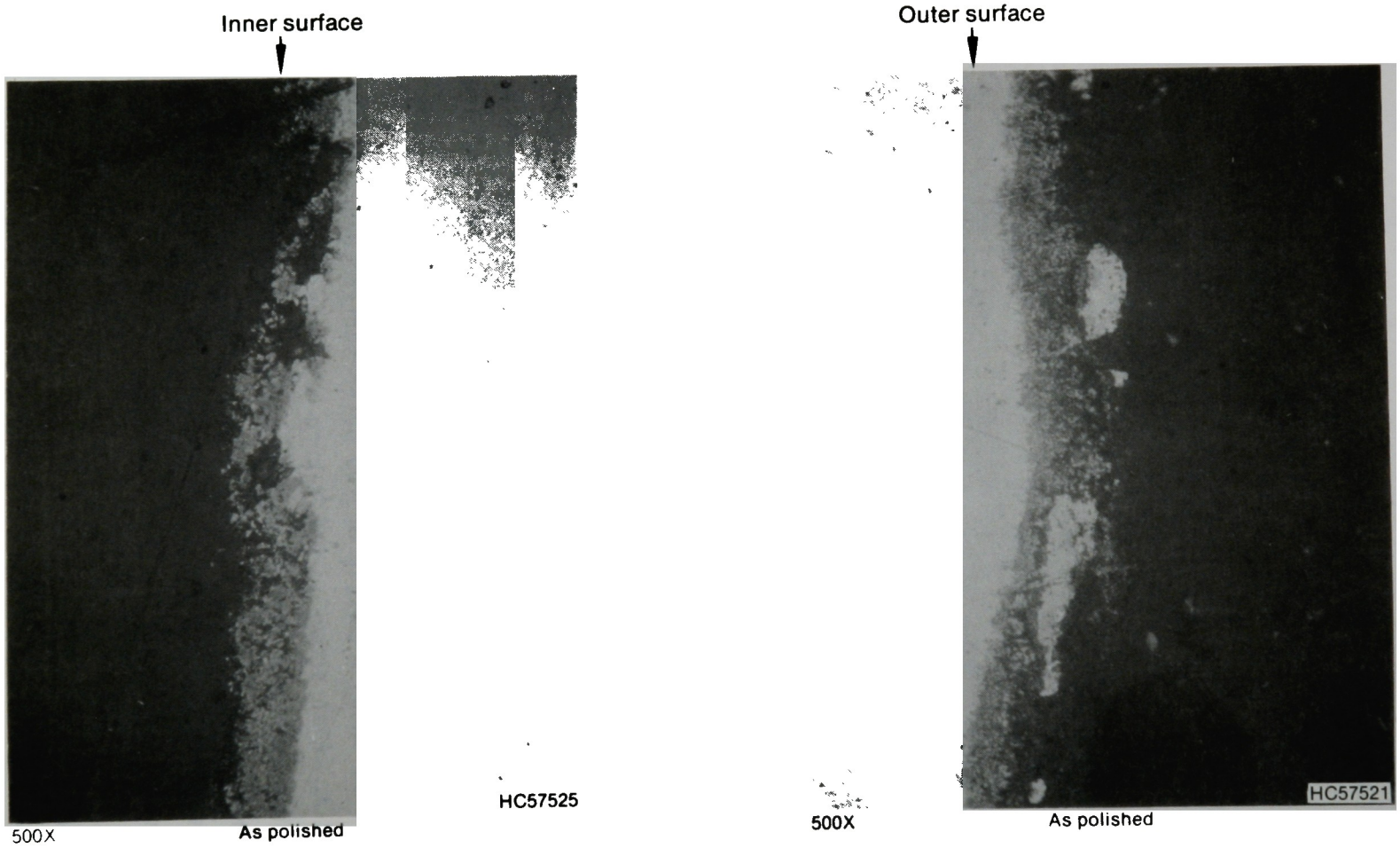

Figure 14. High-magnification photomicrographs showing the typical appearance of inner and outer surface deposits on Specimen 1-1 (note absence of metallic particles in inner surface deposit).

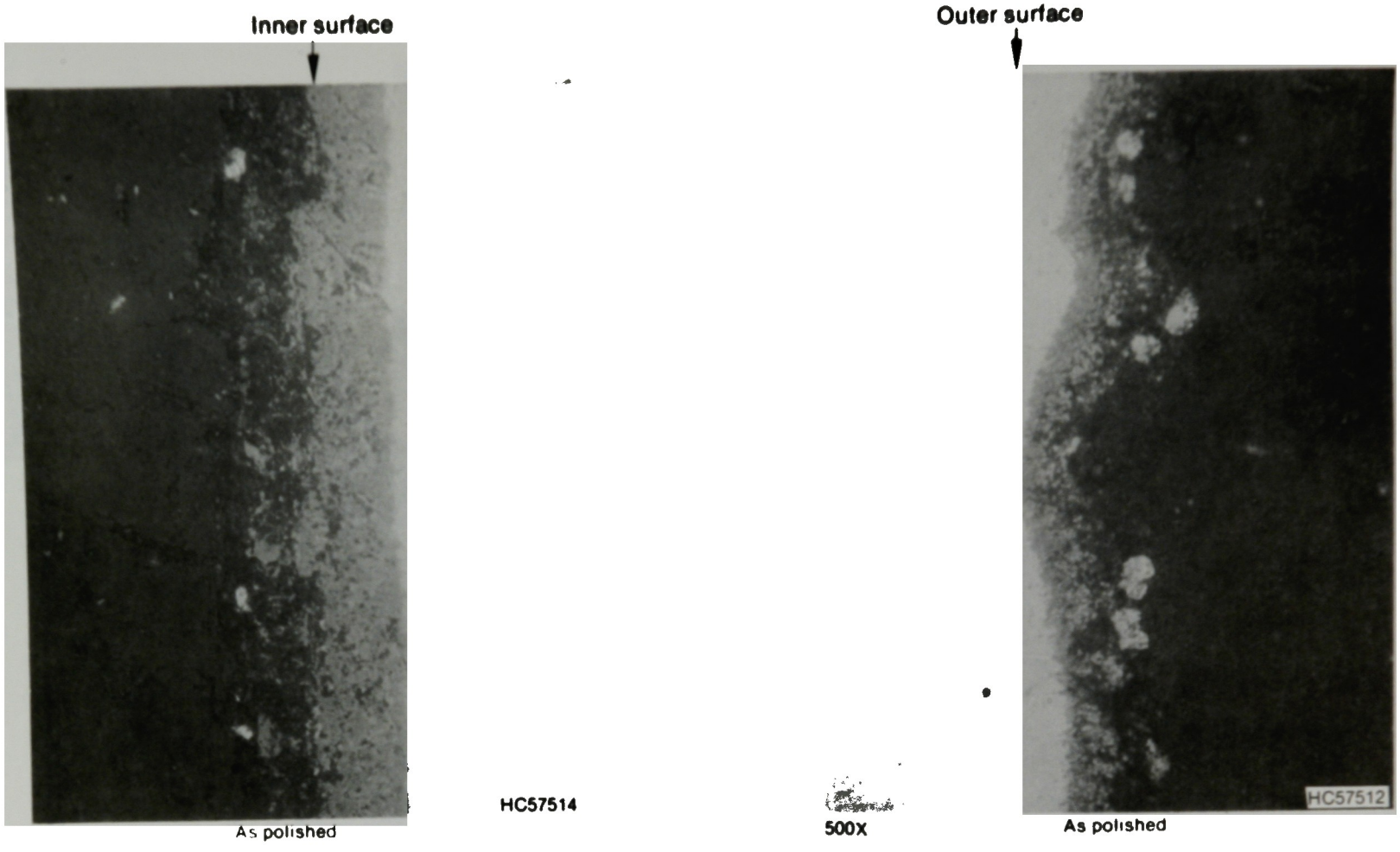

Figure 15. Typical appearance of inner and outer surface deposits on Specimen 5-6.

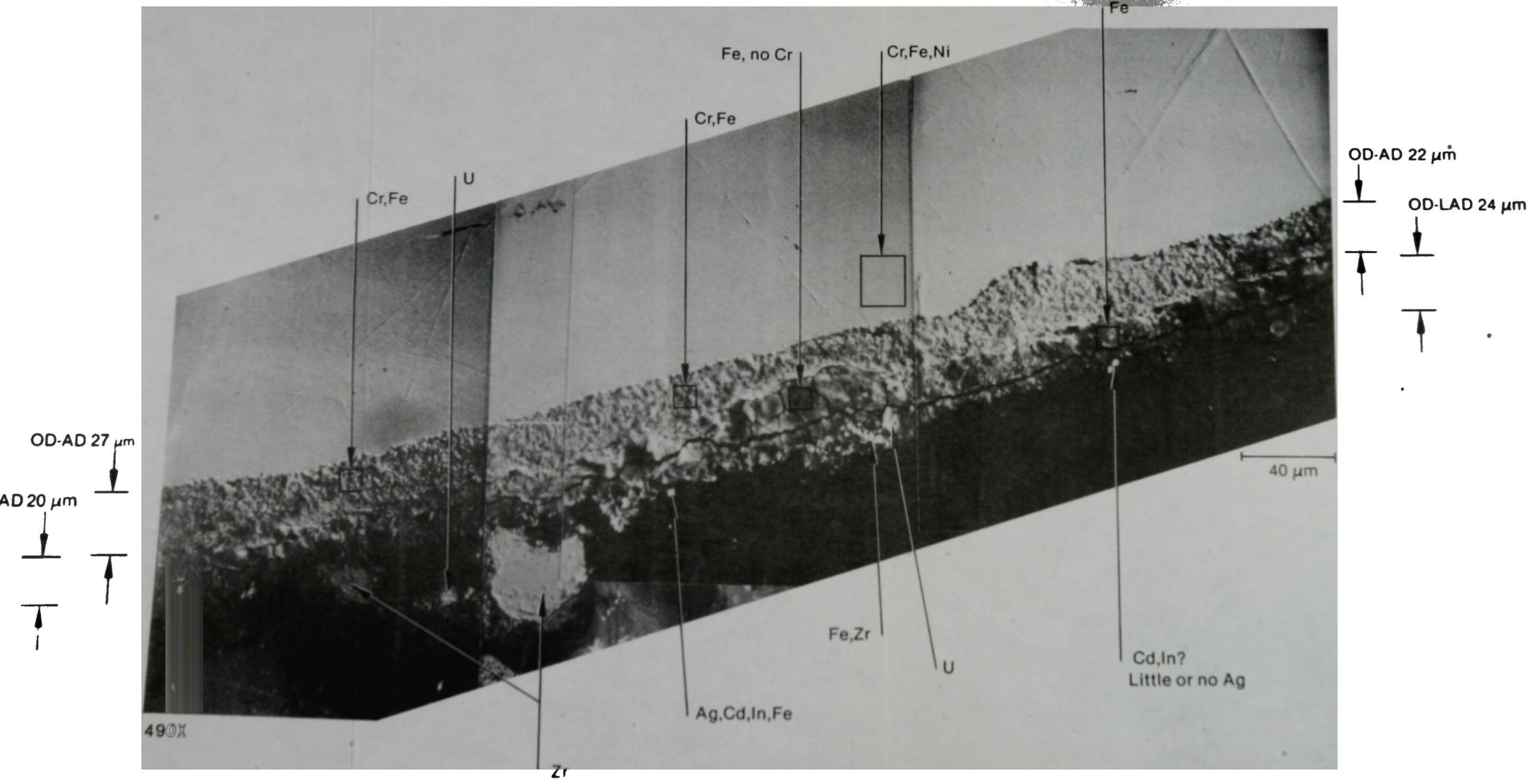

Figure 16. Mosaic of outer surface deposits on Specimen 2-3, showing elements present in each area analyzed with EDAX.

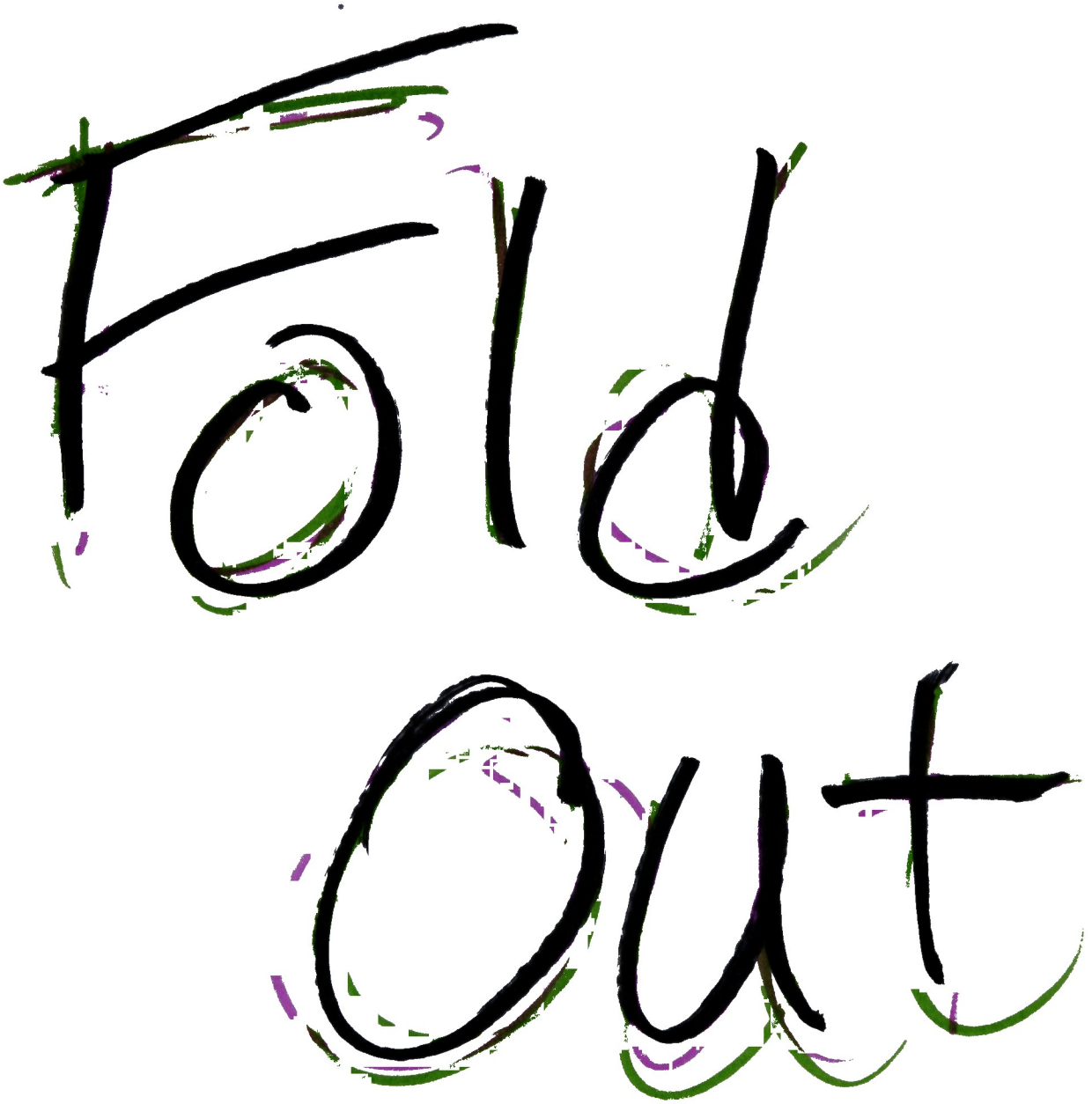
Fold
Out

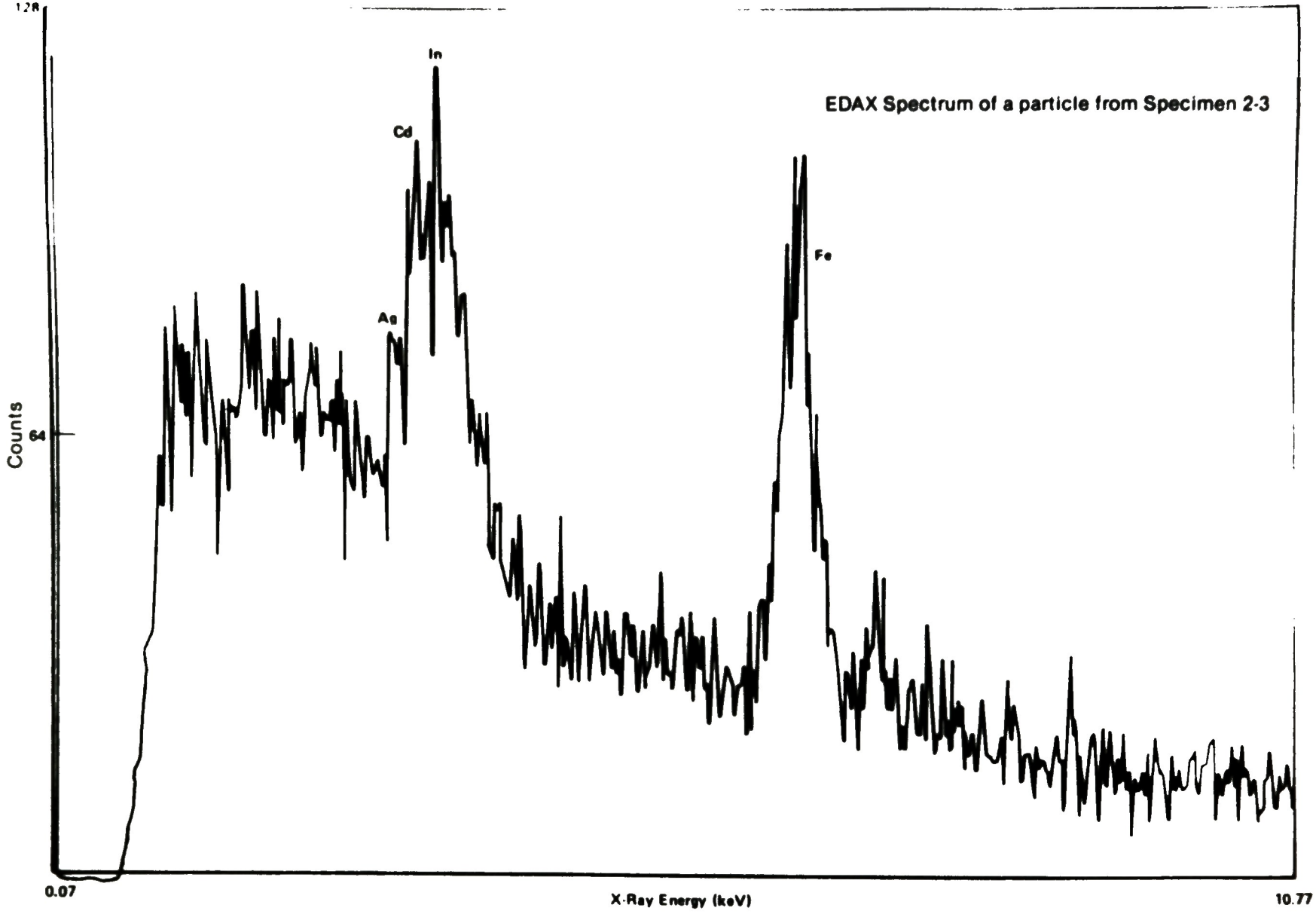

Figure 17. Typical EDAX spectrum for a particle from Specimen 2-3.

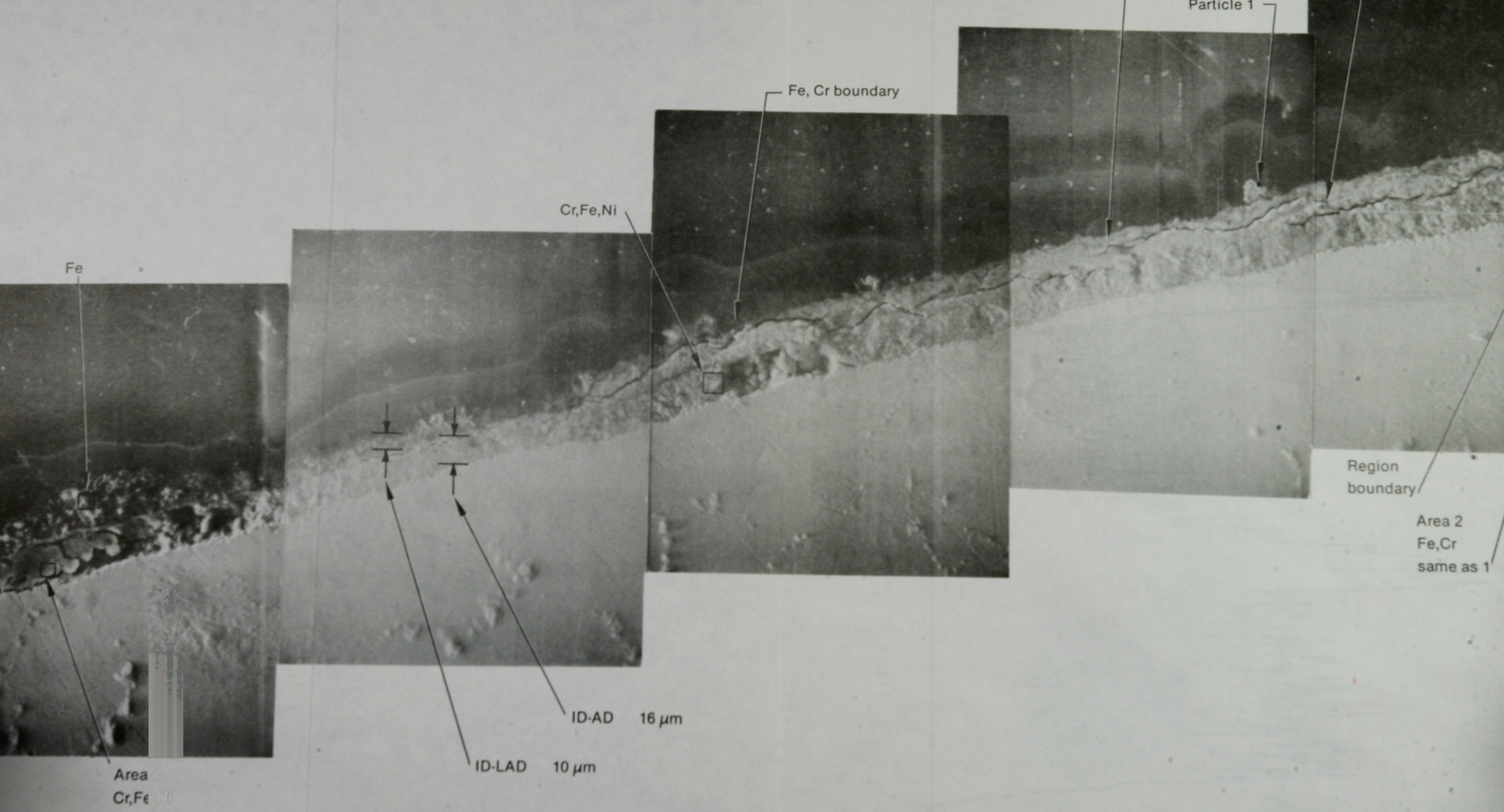

Figure 18. Mosaic of inner surface deposit on Specimen 2-3, showing elements present in each area analyzed with EDAX.

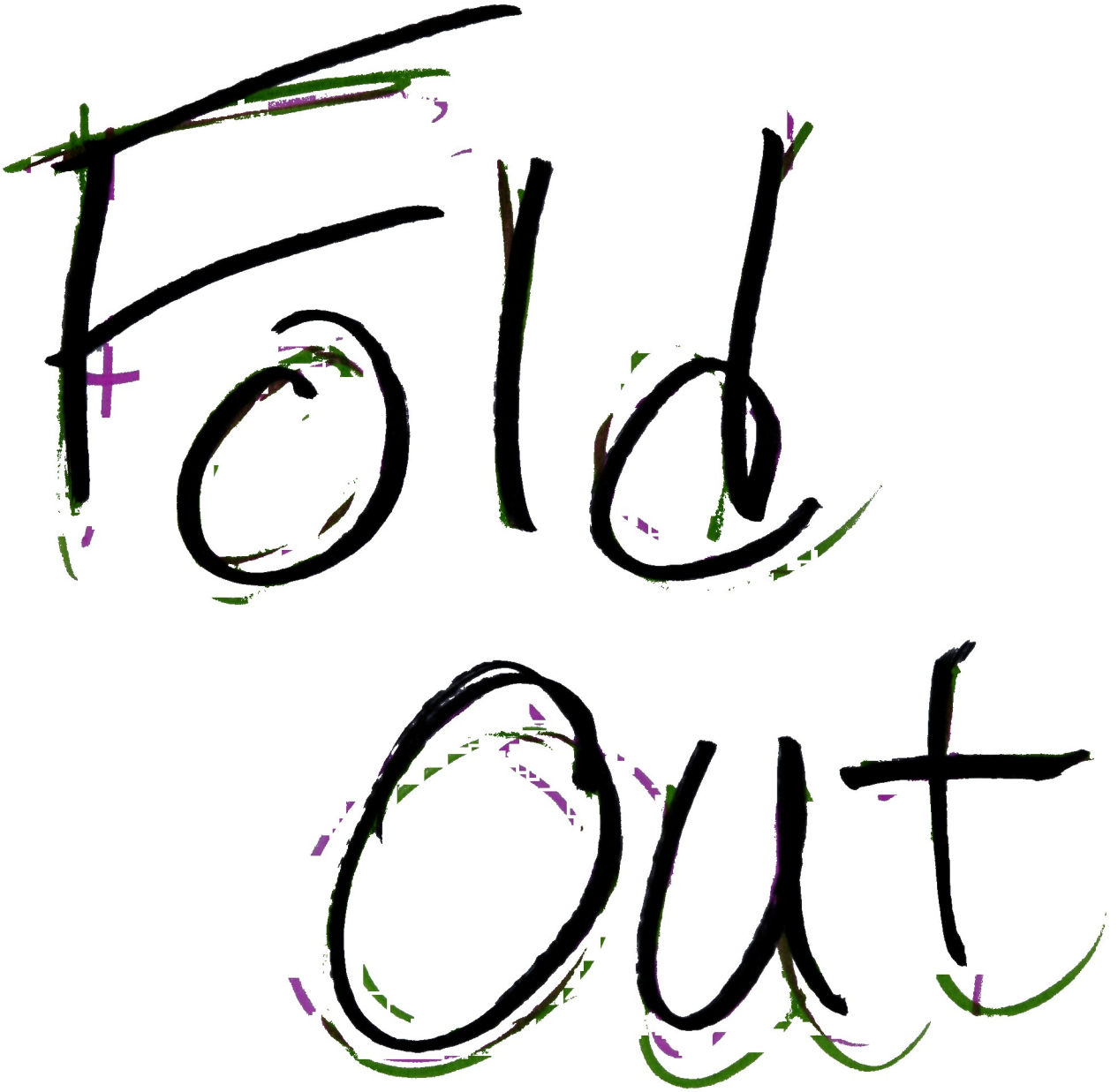
Fold
Out

Figure 19 shows the outer surface deposits on Specimen 5-6 and representative areas analyzed with EDAX. Figures 20 and 21 show typical x-ray spectra obtained at two different locations of Specimen 5-6.

Results of microchemical analyses using SEM/EDAX are as follows:

- No fission product cesium was detected in the deposits. Even though the primary source of radioactivity in the LST section was found to be cesium, its concentration apparently was not high enough to be detected by EDAX. The limit of detectability for cesium is estimated to be about 0.2 wt%.

- About 50 particles were analyzed. Very few, isolated particles containing uranium were observed on the outer surfaces.

- The metallic particles (globules) observed at the bottom end and on the outer surfaces appeared to contain Ag, In, and Cd. The compositions of these particles varied widely.

- Most of the inner surface deposits appeared to contain varying amounts of iron and chromium.

- The adherent layer on the OD surfaces ranged in thickness from about 15 to 40 μm, and on the ID surfaces from about 15 to 30 μm.

- The loosely adherent layer on the OD surfaces ranged in thickness from about 4 to 35 μm. On the ID surfaces, the layer was barely observable in many areas and as thick as 20 μm.

In addition to the metallographic specimens, one small sample containing outer surface deposits also was examined using SEM. Figures 22 and 23 show the typical appearance of the surface layer. The features are consistent with the appearance of the porous, uneven thickness of the deposit observed in the metallographic specimens. X-ray images for Ag were

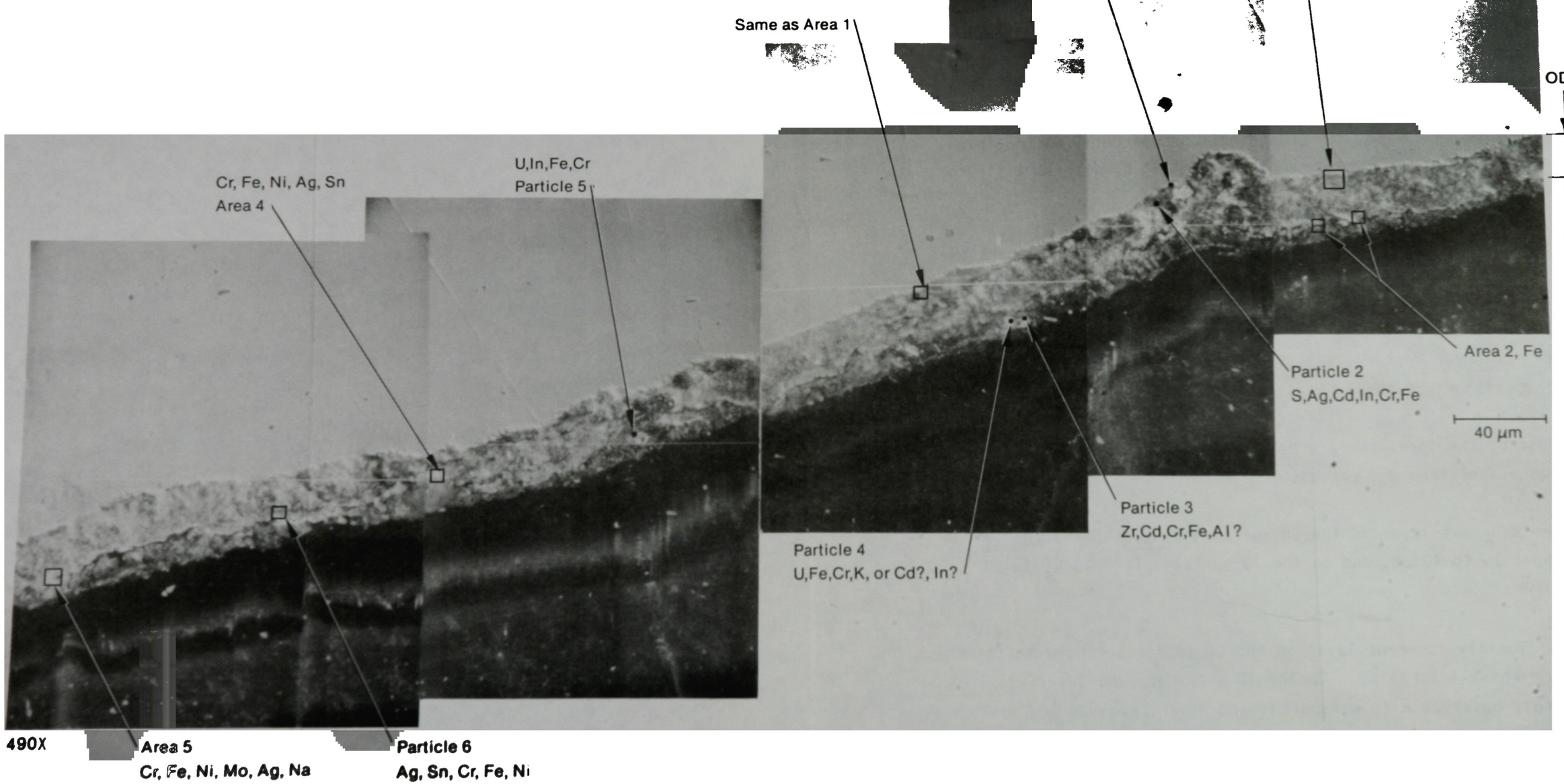

Figure 19. Mosaic of outer surface deposits on Specimen 5-6, showing elements present in each area analyzed with EDAX.

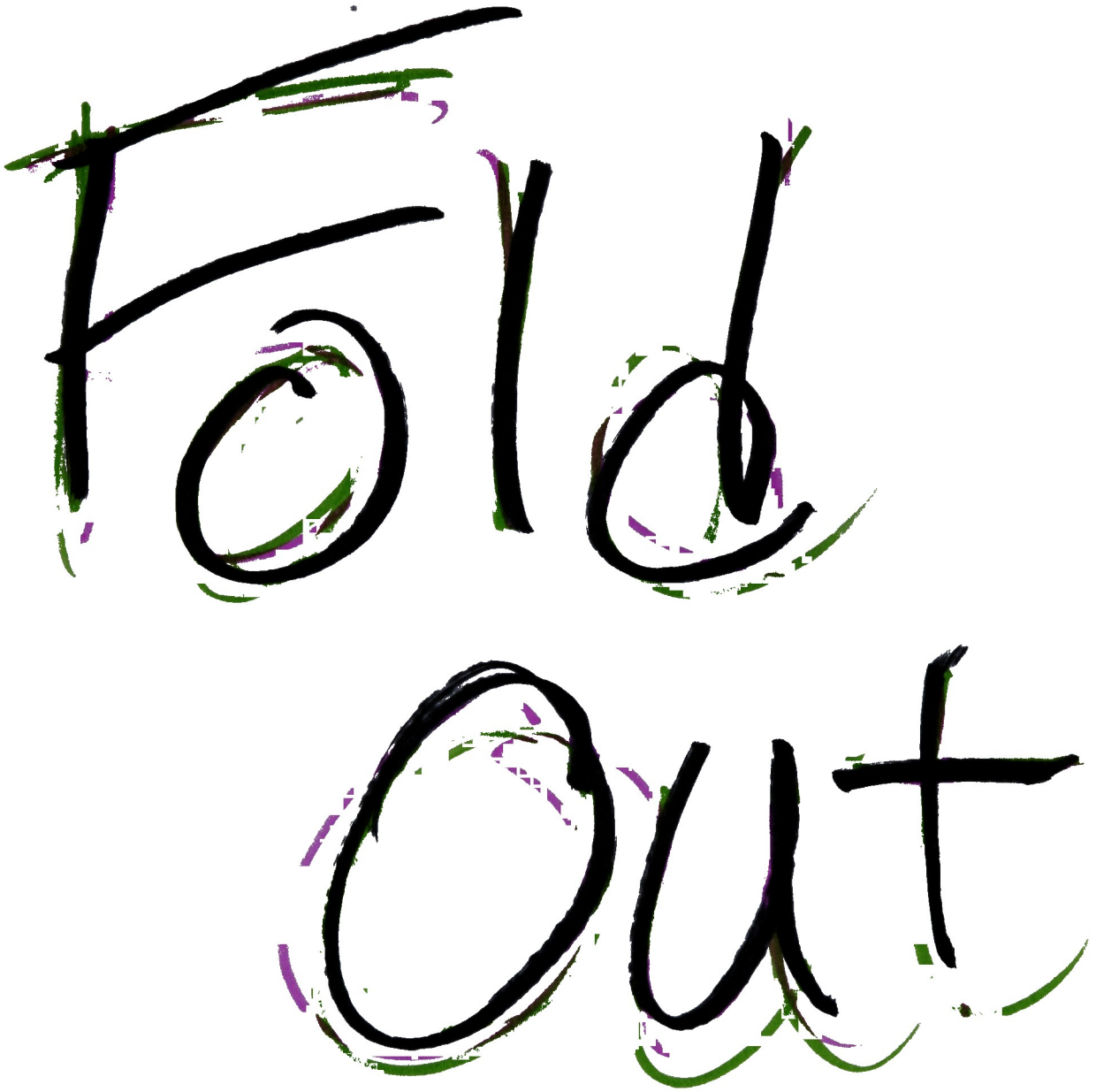
Fold
Out

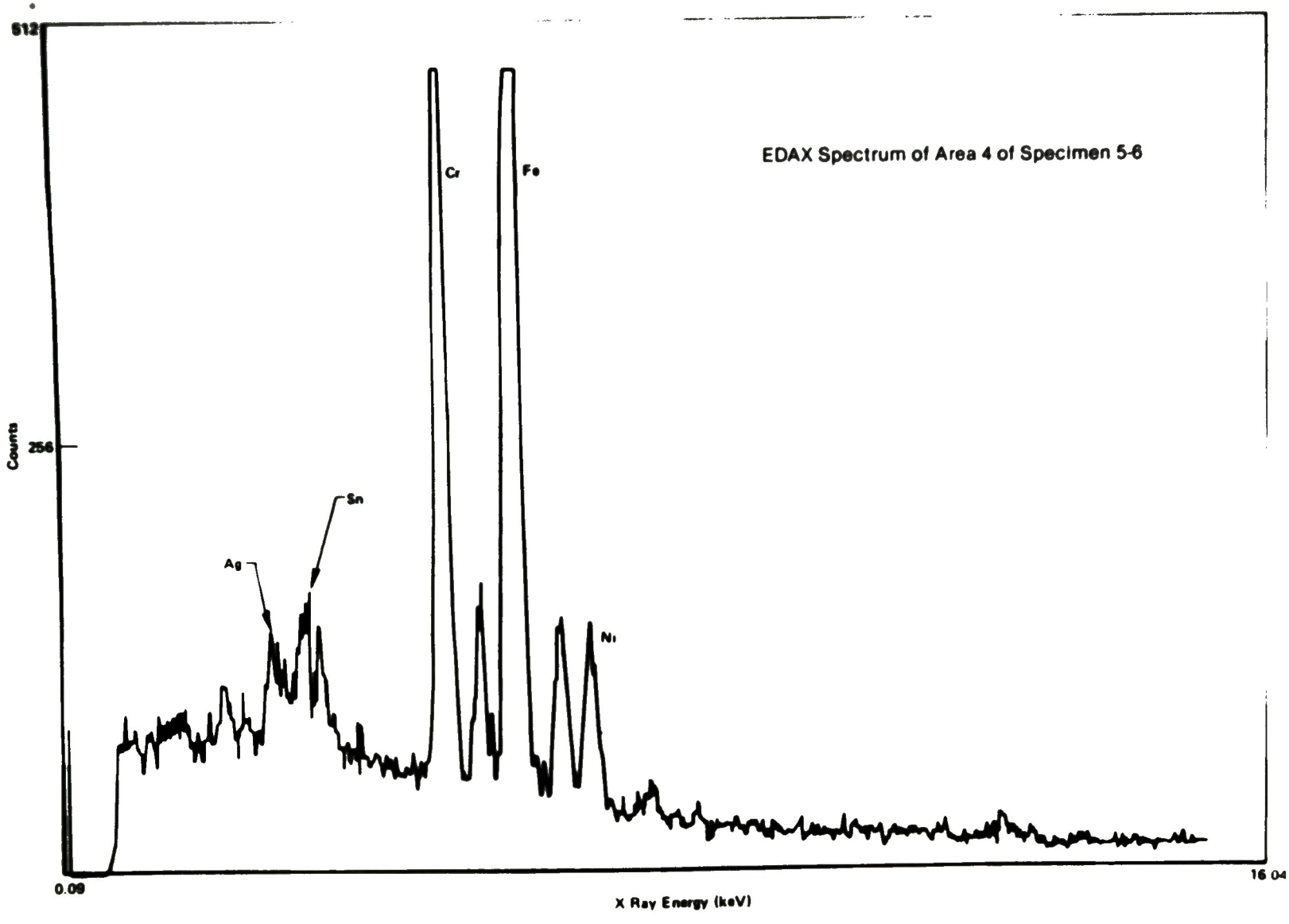

Figure 20. Typical EDAX spectrum of an area of Specimen 5-6.

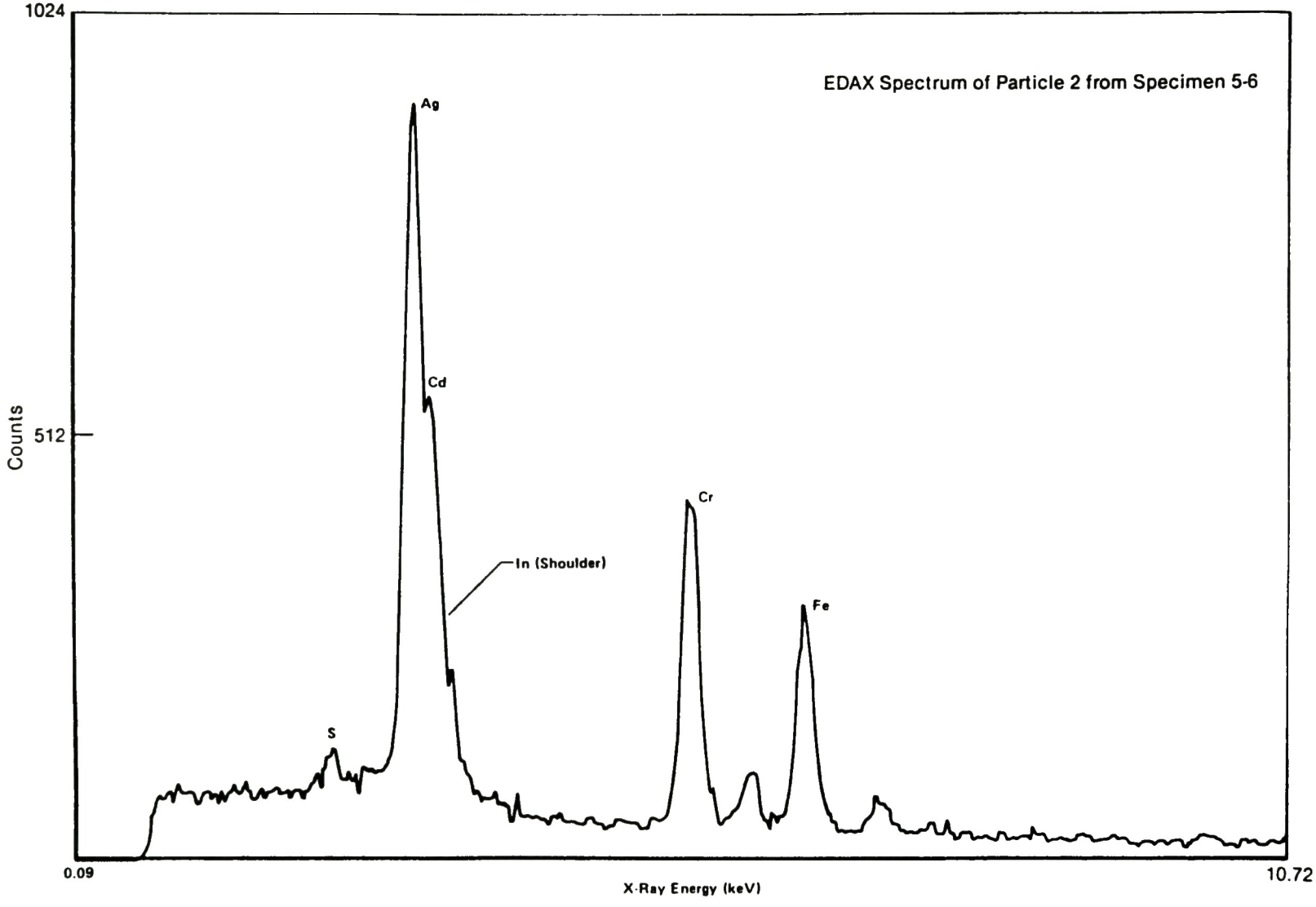

Figure 21. Typical EDAX spectrum of a particle found on Specimen 5-6.

240X

Figure 22. Appearance of the outer surface deposit on a sample from Specimen 5-1.

525X

Figure 23. Higher-magnification view of the outer surface deposit on a sample from Specimen 5-1.

obtained at several different locations. Figure 24 shows the appearance of the deposit and the x-ray map for silver for that location. It appears that silver is present in localized areas of the deposit, as well as in metallic particles.

2.4.2 Temperature History Evaluation

Metallographic examinations were performed on a specimen that was removed from the LST section in order to determine the temperature history of the section during the TMI-2 accident. There are two ways to determine the possible thermal history: (1) examine the microstructure for evidence of sensitization (carbide precipitation at the grain boundaries) and (2) measure the grain size of the stainless steel.

For microstructural examination, the specimens were prepared according to standard metallographic procedures. First, the specimen was etched electrolytically in a solution containing 10-wt% oxalic acid in distilled water, in accordance with Practice A in ASTM Standard Specification A262, "Detecting Susceptibility to Intergranular Attack in Stainless Steel." The photomicrograph in Figure 25 shows that the microstructure was "ditched," indicating sensitization, or carbide formation at the grain boundaries of the specimen. Sensitization of Type 304 stainless steel occurs in the temperature range of approximately 500 to 950°C (930 to 1740°F), with shorter times required to produce sensitization at the higher temperature. Since the oxalic acid etchant also attacks the matrix, reliable measurements of the size of the carbides could not be made. The metallographic specimen was repolished and etched electrolytically in a solution containing 80 parts phosphoric acid and 20 parts water. This etchant attacks only the carbides, not the matrix. Figure 26 is a photomicrograph of the carbide grain-boundary network. However, since the magnification of the light microscope is limited, the size of the carbide particles could not be measured readily. Thus, the specimen was examined using the SEM. Figure 27 is an SEM photomicrograph of a typical grain-boundary area. The thickest carbides seen in this photomicrograph measured approximately 2 μm.

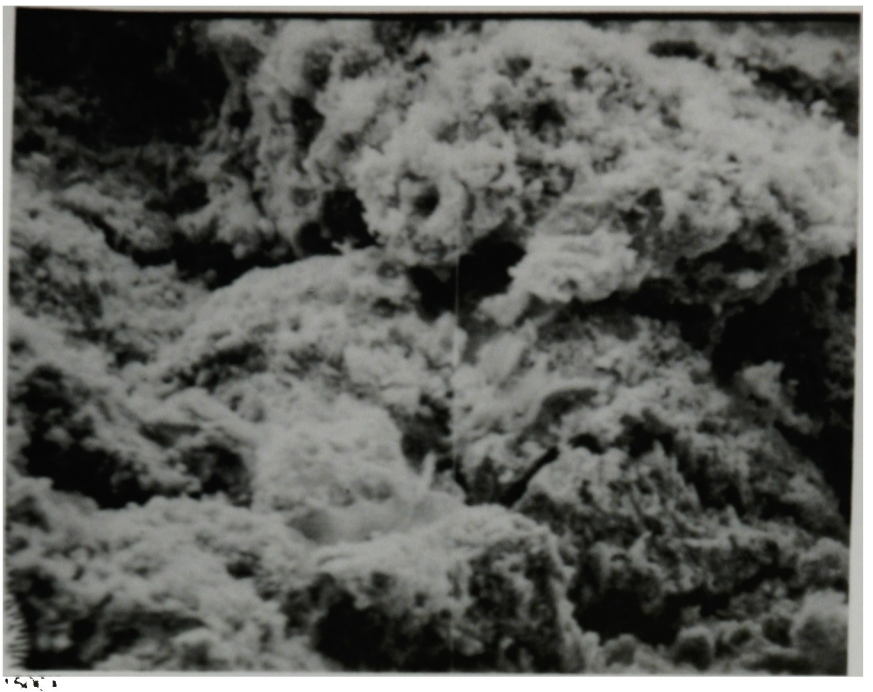

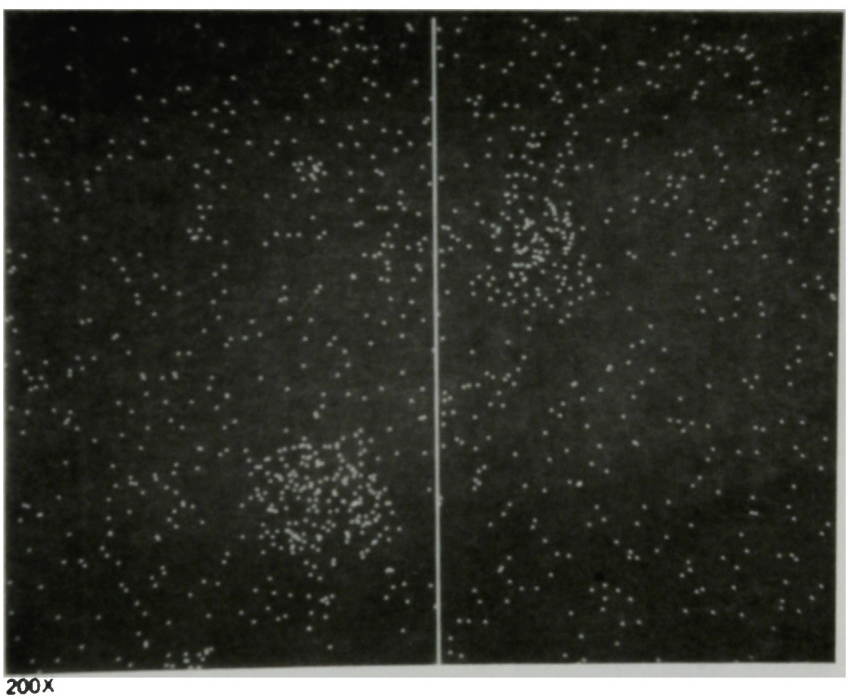

Figure 24. X-ray map for silver, showing localized enhancement in silver concentration in the loosely adherent deposit of Specimen 5-1.

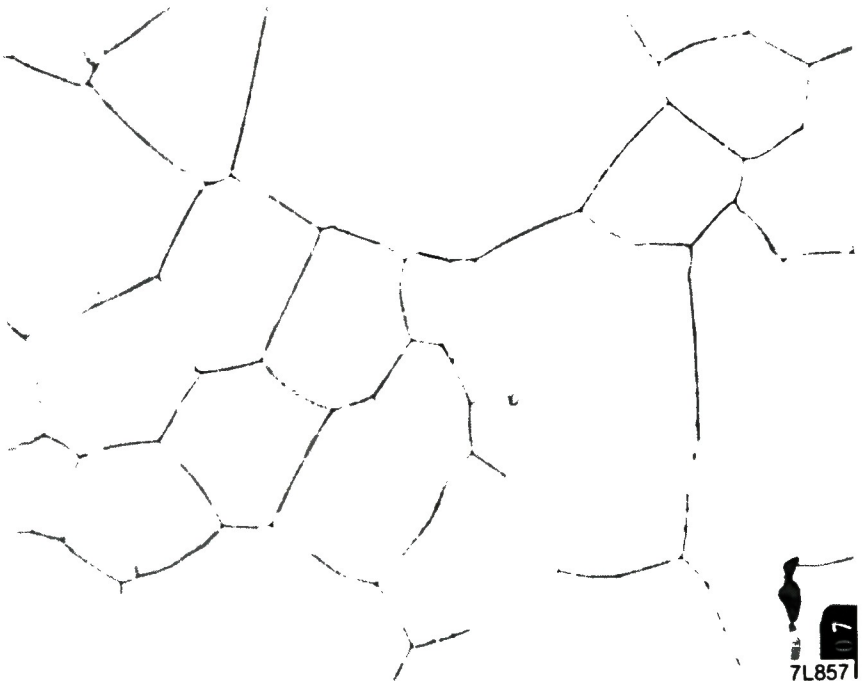

Figure 25. Photomicrograph of a sample from Specimen 2-2 of the LST section, showing the "ditched" structure from ASTM A262 Practice A test for detecting susceptibility to intergranular attack in stainless steel.

8L539

1000X

80-phosphoric acid, 20-water
electrolytic

Figure 26. Photomicrograph of a sample from Specimen 2-2, showing distribution of the grain boundary carbides in the LST material.

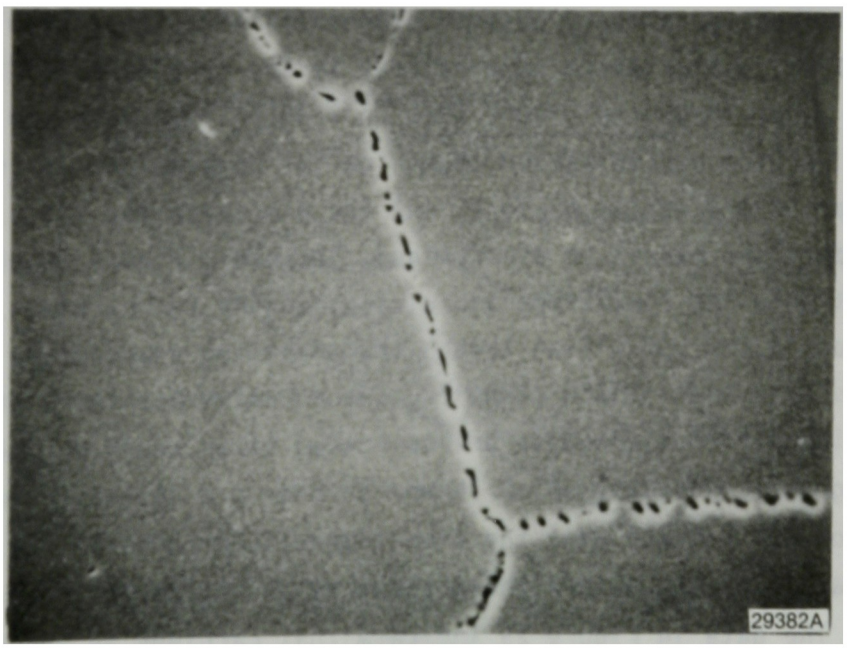

5000X

80-phosphoric acid 20-water
electrolytic

Figure 27. SEM photomicrograph of a sample from Specimen 2-2, showing the locations and sizes of the grain boundary carbides.

The grain size of the stainless steel then was measured. The grain size of stainless steel typically is related to the annealing temperature, with higher temperatures producing larger grain sizes. Typical annealing temperatures for Type 304 stainless steel are 1010 to 1121°C (1850 to 2050°F). Figure 28 shows that the grain size of the LST material is ASTM No. 5, which is a typical grain size for Type 304 stainless steel that was annealed in this temperature range. The results indicate that the temperature of this component did not exceed the pre-service annealing temperature.

Results of the metallographic examinations indicate that the LST must have experienced temperatures in the range of from 500 to 950°C (930 to 1740°F) for some period of time during manufacture or service, because grain-boundary carbides form in this range. These temperatures are above the 288 to 304°C (550 to 580°F) temperature range of the reactor during normal operation. However, since the pre-service processing history of the LST was not available, it is not known whether the LST reached this temperature during the TMI-2 accident. If the LST was supplied in the annealed-and-quenched condition (as is the case for most Type 304 stainless steel used in reactor primary system components) then these results show that the LST was subjected to temperatures in the carbide-precipitation temperature range of 500 to 1740°C (930 to 1740°F). Because the specific kinetics of carbide precipitation depend on the chemical composition of the alloy, its prior processing history, and the precipitation sites, the precise temperature cannot be ascertained. However, Figure 29 does provide some insight into the time-temperature relationship for carbide precipitation in the LST. Even though the annealing temperature of the LST probably was less than 1250°C (2280°F), the relative positions of the curves for the different carbide precipitation sites would be the same. The metallographic results, which showed carbide precipitation in the grain boundaries only, indicate that the time-temperature combinations that the LST could have experienced are those shown by the hatched area in Figure 29. The data in Figure 29 indicate that carbides in the grain boundaries could only be produced by short times at high temperatures or long times at lower temperatures.

Figure 28. Photomicrograph of a sample from Specimen 2-2, showing the grain size to be ASTM No. 5.

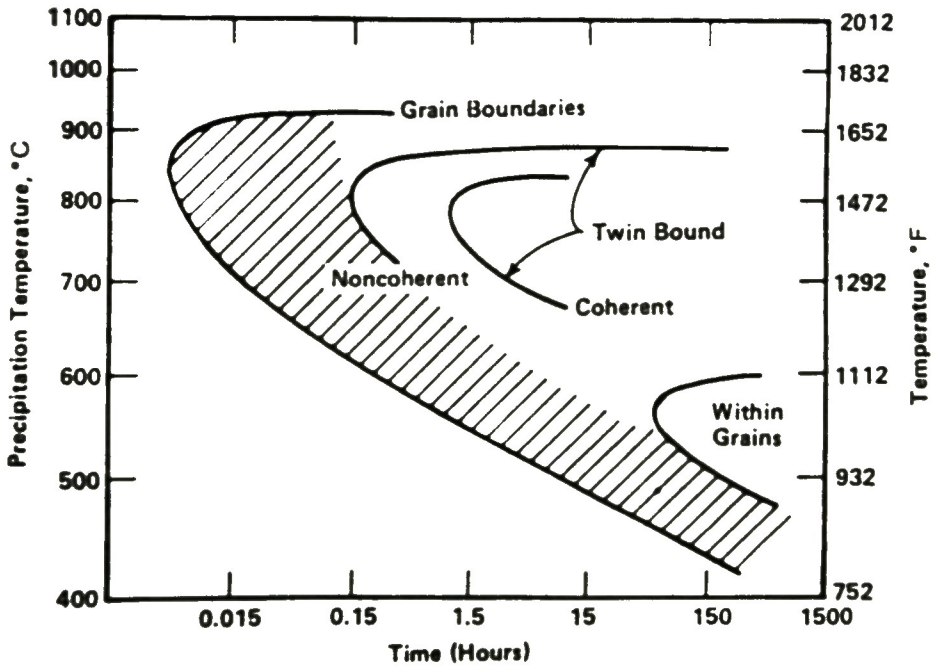

Figure 29. Precipitation kinetics of $M_{23}C_6$ carbide in a Type 304 stainless steel containing 0.05% carbon that was originally quenched from 1250°C (Reference 4).

The grain size of the material from the LST was judged to be ASTM No. 5, which is considered typical for Type 304 stainless steel that has been annealed in the temperature range from 1010 to 1121°C (1850 to 2050°F). The maximum annealing temperature consistent with limited grain growth generally is considered to be about 1095°C (2000°F). If the material had been heated to above 982°C (1800°F) for any appreciable time, the carbides should have been dissolved; however, judging by Figure 29, carbides observed in the microstructure could have precipitated if the material were cooled to below approximately 815°C (1500°F) within about one hour after the cooling began. Otherwise carbides probably would have been observed on twin boundaries also.

Hardness testing of the LST material would provide little additional information on its thermal history, unless the material had been supplied in a cold-worked condition. The reason is that austenitic stainless steels cannot be hardened to any great extent by heat treatment, although they can be hardened appreciably by cold work.[4] Also, the highly localized precipitation of chromium carbides at the grain boundaries and the attendant depletion of chromium in a very thin grain-boundary zone have no significant effects on the overall hardness of the material, as determined by macrohardness methods, such as Rockwell or Brinell tests. Thus, if the LST material was supplied in the annealed condition, the effect of carbide precipitation during the thermal transient would not be expected to alter the hardness significantly.

2.4.3 I-129 Analysis

Five samples were analyzed for I-129, with repeat analyses performed on one sample to assess the effectiveness of the technique in separating iodine from the sample. The AD samples were in the form of small metal samples with either the OD or ID layers removed, and the LAD material was in the form of scraped powders. One sample (Sample 6-1.2 ID-AD) was analyzed by adding I-125 and iodine carrier to the sample, then reacting it with H_2SO_4, HNO_3, HCl, NaClO, and NH_4HF_2 in a closed system. Iodine-129 then was determined by measuring the chemical iodine yield and determining the I-125/I-129 ratio. Because the chemical yield was so low

(0.6%), all other measurements were performed using a hot hydrogen bake out procedure followed by chemical yield determination and mass spectroscopy. Sample 6-3.1 ID-AD was analyzed twice to estimate if the bake-out procedure was actually removing most of the I-129. The second analysis resulted in a measurement of only 2% of the I-129 value determined during the first analysis. The much lower value determined the second time suggests that the iodine is effectively removed from the deposits by the bake-out techniques. Table 11 lists the results of the I-129 analysis, including those of the repeated analysis. The results are listed in terms of atoms per unit mass or unit area. To convert to μCi, multiply the value in the table by the specific activity of I-129, which is 3.74×10^{-20} μCi/atom. As can be seen, the I-129 activity per unit area in the OD-AD is about two times greater than that of the ID-AD. This is close to the ratio of the cesium activities between the OD and ID-AD layers, as discussed in Section 2.3.4. For the LAD material, the scraped area was estimated and the atoms/cm^2 calculated. The calculated values also are listed in Table 11.

TABLE 11. RESULTS OF THE I-129 ANALYSIS

Sample	Chemical Yield (%)	Concentration (atoms/mg)	Concentration (atoms/cm^2)	Error (%)
6-1.2 ID-AD	0.6	--	1.3×10^{14}	3.2
6-3.1 ID-AD	77.0	--	1.0×10^{14}	2.0
Repeat of above	67.0	--	1.8×10^{12}	3.1
6-2.2 OD-AD	48.0	--	2.1×10^{14}	4.7
ID-LAD	74.0	2.6×10^{13}	3.4×10^{12}	9.4
OD-LAD	56.0	9.6×10^{13}	1.2×10^{13}	7.5

3. EVALUATION OF RESULTS

It is intended that acquisition of data from TMI-2 will provide the information necessary to gain insights into a number of key issues on severe accident behavior and accident source terms. These issues include the following: (a) flow circulation within the upper plenum and back into the core region; (b) heat transfer between gases exiting the core and upper plenum structures; (c) release and transport of fission product vapors and inert structural and control material vapors from the core, and their condensation to form aerosols; (d) deposition of fission product vapors, control rod material vapors, and aerosols on upper plenum structures; and (e) extent of oxidation of upper plenum structures.

It is too much to expect that examination of upper plenum surfaces can provide a clear, unambiguous record of all these phenomena. The structures had been submerged in water for several years. Some of the boundary conditions that existed during the accident are not well known. Furthermore, examination of a single component, the leadscrew support tube, cannot resolve these issues but can only add to the growing body of data. In particular, it should be recognized that because of its location in the upper dome region, it is expected that the LST saw relatively limited coolant flow. Indeed, because the LST is dead-ended, the inside surface should have seen virtually no flow during the accident.

Results obtained from examining the LST are largely consistent with data obtained previously from pieces of leadscrew. Of particular interest are the conditions that occurred in the upper plenum region during the time of core uncovery, when the upper plenum was subjected to high temperature gases, fission product vapors, and aerosols. It is hoped that examination of the upper internals above the core will provide insight into the issues discussed above.

The following observations can be made based on the results of this examination and their relationship to other studies:

- The total mass of fission products deposited on the LST represents a very small fraction of the mass of fission products released from the core. It should be recognized that the extent of deposition could have been higher during the accident but may have been decreased by subsequent washing.

- Some corrosion of upper plenum structures did occur during the high temperature transient portion of the accident. Quantitative evaluations should be made after the upper plenum examinations are completed.

- Data from metallurgical analysis of the LST are consistent with estimates of upper plenum temperatures obtained from the leadscrews; however, uncertainties in the estimated temperature of the LST are too large to add much to the state of knowledge.

- Control rod materials (Ag, In, and Cd) and tin from the cladding vaporized and condensed on the upper plenum structures. The total mass represented by deposition on the LST appears to be small. Deviations from the as-fabricated Ag-In-Cd composition observed in the droplets suggest fractioning of the alloying elements in the molten or vapor state.

- Droplets of molten control rod material apparently were carried to the upper dome region by steam at flow rates that were substantially higher than the quasi-steady boiloff rate from the core. Further analyses are necessary to determine whether these results have implications for control rod failure modes or melt-coolant interactions.

These conclusions are based on the examination of the LST alone. It must be recognized that an integrated evaluation of <u>all</u> data currently available may well lead to different conclusions.

4. RECOMMENDATIONS FOR FOLLOW-ON WORK

The results presented herein were obtained from examining the bottom 9.5-cm section of the H8 leadscrew support tube. Additional information regarding radionuclide and core material transport, as well as temperature history, could be obtained by performing similar studies on additional sections from higher in the plenum region. Additional studies would provide better understanding of the nature of deposits.

A search for the pre-service heat treatment history of the LST should be undertaken. Findings from the search could be correlated with this study to deduce time-temperature exposure during the accident. However, if information on the pre-service condition is not available, other experiments can be performed. Heat treatment experiments on remaining samples of the LST section could be performed to duplicate the observed microstructural carbide precipitates. This would help narrow the estimates of maximum temperature exposure.

The metallographic or additional prepared samples could be chemically etched to reveal the presence of materials with ceramic characteristics. If present and identified, the ceramic areas probably could be separated for further structural and elemental analysis.

Some of the larger individual metallic particles observed at the bottom of the LST section could be separated, examined using SEM/EDAX, and analyzed chemically to determine the nature of the particles and the elemental ratios of Ag, In, and Cd.

The individual microscopic particles embedded in the deposit layers could be analyzed semi-quantitatively using EDAX. The particles have shown diverse elemental compositions. With more advanced data reduction techniques, the elemental ratios could be determined more accurately.

Finally, in this study, no attempt was made to identify the nature of the yellow-orange deposits observed on some surfaces of the LST section.

this could be accomplished in a follow-on study by removing the deposits with adhesive tape and analyzing the removed material using ESCA.

All of the above suggestions are intended to supplement and optimize the information obtained thus far. It is, however, recognized that the small section of LST available for examination limits the extent of extrapolation of results to the overall accident sequence.

5. REFERENCES

1. K. J. Hofstetter, H. Loewenschuse, V. F. Baston, Chemical Analyses and Test Results of Sections of the TMI-2 H-8 Leadscrew, TPO/TMI-103, Rev. 0, January 1984.

2. G. M. Bain and G. O. Haynes, Initial Examination of the Surface Layer of a 9-Inch Leadscrew Section Removed From Three Mile Island 2, EPRI NP-3407, January 1984.

3. L. A. Currie, "Limits for Qualitative Detection and Quantitative Determination," Analytical Chemistry, 40, 586, 1968.

4. D. Pechner and I. M. Bernstein, Handbook of Stainless Steels, New York: McGraw-Hill, 1977, pp. 20-25.